

***Microseismic Monitoring of a Room and  
Pillar Retreat Coal Mine in  
Southwest Virginia***

William Jennings Conrad

*Thesis submitted to the faculty of the Virginia Polytechnic Institute and State  
University in partial fulfillment of the requirements for the degree of*

Master of Science  
In  
Mining & Minerals Engineering

Erik C. Westman, Chairman

Mario G. Karfakis

Kramer D. Luxbacher

03 December 2015

Blacksburg, VA

Keywords: Microseismic, retreat mining, coal, ground control, stress

# ***Microseismic Monitoring of a Room and Pillar Retreat Coal Mine in Southwest Virginia***

William Jennings Conrad

## ***Abstract***

Ground control, one of the key elements in mine safety, is an issue that warrants continuous improvement in the underground coal industry. The United States experienced over 3,300 injuries and 42 deaths between 2006 and 2012 from the fall of a roof or rib (MSHA, 2015). Out of the underground coal mining methods, room and pillar retreat mining lacks significant research to adequately understand the rockmass behavior associated with the process. A microseismic monitoring system was installed in a retreat mine in Southwest Virginia to provide more information about the changing stress conditions created by retreating and ultimately reduce risk to miners. Microseismicity has been proven to be an acceptable method of monitoring stress redistribution in underground coal mines and assist in explaining rockmass behavior (Luxbacher, et al, 2007). An array of geophones was placed underground along a single retreat panel to record failures due to stress redistribution throughout one panel of retreat. These microseismic events were located, and their moment magnitudes were found. An analysis was completed to observe the redistribution of stress and related gob formation throughout the panel's retreat. Expectations for the gob formation were consistent with the distribution of microseismic events. Over 13,000 microseismic events were found in 1.5 months of monitoring. Approximately 2,800 of these events were well enough located to provide analysis of the changing underground stress conditions from the retreat process. On average, recorded microseismic events during retreat produced a moment magnitude of -0.9, with no events higher than a magnitude of 2.0.

## ***Acknowledgements***

I would like to thank my advisor, Dr. Erik Westman, for his support and direction, not only while completing my master's degree, but throughout my college career. I would also like to thank Dr. Mario Karfakis and Dr. Kray Luxbacher for taking their time to be my committee members. Dan Neilans, from Alpha Natural Resources, and the employees at the studied mine were vital as well for the completion of this research. They went above and beyond to help out in whatever aspect was needed. Finally, I would like to thank my family, fellow graduate students, staff of Virginia Tech's Mining and Minerals Engineering Department, and other friends in their continued support.

This research would not have been possible without the funding from NIOSH's capacity building contract 200-2011-40313. I am grateful that the Office of Mine Safety and Health Research designated funds to educate graduate students to address critical health and safety problems in U.S. mines.

# Table of Contents

Table of Contents .....	iv
List of Figures .....	vi
List of Tables .....	viii
Chapter 1: Introduction .....	1
Chapter 2: Literature Review.....	1
2.1 Room and Pillar Retreat Mining .....	3
2.1.1 Description.....	3
2.1.2 Deep Pillar Recovery.....	4
2.1.3 Retreat Mine Loading.....	4
2.1.4 Pressure Arch Theory .....	7
2.1.5 Subsidence .....	8
2.1.6 Design Parameters.....	9
2.1.6.1 Global Stability.....	9
2.1.6.2 Pillar Design .....	12
2.1.6.2.1 ARMPS.....	12
2.1.6.2.2 LaModel.....	13
2.1.6.3 Local Stability.....	14
2.1.6.3.1 Cut Sequences .....	14
2.1.6.3.2 Final Stump.....	14
2.1.6.3.3 Mobile Roof Support.....	15
2.1.6.4 Major Parameters Contributing to Ground Control Issues.....	15
2.1.6.4.1 Depth of Cover.....	15
2.1.6.4.2 Roof Rock Quality .....	15
2.1.6.4.3 Floor Quality .....	17
2.1.6.4.4 Groundwater .....	17
2.1.6.4.5 Multiple-Seam Interaction .....	17
2.2 Microseismic Monitoring .....	18
2.2.1 Purpose .....	18
2.2.2 Rock Failure Modes .....	19
2.2.3 Formation of Microseismic Events .....	21
2.2.4 Moment Magnitude .....	22
2.2.5 Seismicity Relating to Ground Failure .....	23
2.2.6 Shear and Tensile Fracture Signatures .....	23
2.2.7 Wave Propagation Path Effects.....	24
2.2.8 Processing Levels .....	24
2.2.9 Chain Reaction Failures.....	25
2.2.10 Limitations .....	26
2.2.11 Microseismic Modeling .....	27

2.2.12 Past Mining Studies and Assessments.....	27
2.2.12.1 Hard Rock Monitoring .....	28
2.2.12.2 Longwall Coal Mine Monitoring .....	28
2.2.12.3 Retreat Coal Mine Monitoring.....	29
Chapter 3: Microseismic Monitoring of a Southwest Virginian Room and Pillar Retreat Coal Mine .....	32
3.1 Abstract.....	32
3.2 Introduction.....	32
3.3 Site Description.....	34
3.3.1 General Description.....	34
3.3.2 Panel Geology .....	36
3.4 Seismic Monitoring Equipment and Installation.....	40
3.5 Data Collection.....	41
3.6 Data Processing .....	43
3.7 Monitoring Results .....	45
3.7.1 Panel 2D Retreat .....	45
3.7.2 Panel 2E Development Results .....	52
3.8 Monitoring Analysis .....	55
3.8.1 Panel 2D Retreat Analysis .....	55
3.8.2 Panel 2E Development Analysis .....	61
3.9 Obstacles .....	64
3.10 Conclusions .....	66
3.11 Future Work .....	67
Chapter 4: Summary of Results and Conclusions .....	69
4.1 Results and Conclusions .....	69
4.2 Future Work and Recommendations .....	70
References .....	73
Appendix A: Source Parameter Formulas .....	76
Appendix B: Estimated Timing .....	77
Appendix C: Event Rate Comparison T-Test (3/02-3/08 and 3/11-3/15).....	78
Appendix D: Descriptive Statistics of Processed Events .....	82

# List of Figures

Figure 1: Injuries (FAT, NFDL, NDL) due to the fall of a roof or rib between 2006 and 2012 (MSHA, 2015). .....1

Figure 2: Loadings applied to a retreat panel (after ARMPS, 2013). .....6

Figure 3: Abutment load distribution to the active mining zone (after Mark, 1990). .....7

Figure 4: Typical retreat panel loading model with barrier pillars and pressure arch (after ARMPS, 2013). .....8

Figure 5: Mining subsidence profile (after Ren & Li, 2008). .....9

Figure 6: General progression of roof failure for high horizontal stress (after Iannacchione et al., 2005). .....20

Figure 7: Typical waveforms from naturally occurring events (top three) and .....22

Figure 8: Impact of installation direction on a uniaxial geophone. ....25

Figure 9: Injuries (FAT, NFDL, NDL) due to the fall of a roof or rib between 2006 and 2012 (MSHA, 2015). .....33

Figure 10: Depth of cover contour of Panels 2D and 2E with partial retreat. Geophone locations, cable paths, and Borehole 679 is marked. ....35

Figure 11: Occasional partings in the Jawbone seam in Panels 2D and 2E. ....37

Figure 12: Geologic column of Corehole 679. Total depth: 734 ft. ....38

Figure 13: Geologic column of the immediate roof and floor from Corehole 679. ....39

Figure 14: Geologic influence on the retreat panels. ....40

Figure 15: Mining monitoring period. ....42

Figure 16: Mining progression during monitoring period. ....42

Figure 17: All located microseismic events during Panel 2D retreat. Rectangular outline displays the main cluster of events chosen by hand from the first four days of monitoring. ....46

Figure 18: Microseismic events with a location error of less than 100 ft. during Panel 2D retreat. Rectangular outline displays the main cluster of events chosen by hand from the first four days of monitoring. ....46

Figure 19: Recorded waveform of Trigger 266 on February, 26th 2015. ....48

Figure 20: Event location of Trigger 266 on February, 26th 2015. ....50

Figure 21: Top view of the time progression of microseismic events during the retreat of Panel 2D. Left progression displays all events, while the right progression displays events with a location error of less than 100 ft. ....51

Figure 23: Top and side views of the time progression of microseismic events during the monitoring of Panel 2E’s development. ....54

Figure 24: Event rate (per hour, GMT) for all located events during Panel 2D retreat. ....56

Figure 25: Magnitude verse time (GMT) chart for all located events during Panel 2D retreat. ...	56
Figure 26: Event rate peaks (period 1) with noted times in EST.....	57
Figure 27: Event rate peaks (period 2) with times in EST. ....	58
Figure 28: Magnitude distribution chart for events with an average location error of less than 100 ft. during Panel 2D retreat.....	59
Figure 29: Inter-event distances for events with a location error of less than 100 ft. during Panel 2D retreat.....	60
Figure 30: Time of day plot for all located events during Panel 2D retreat (times in GMT).....	61
Figure 31: Event rate (per hour) for all located events during Panel 2E development.....	62
Figure 32: Time of day plot for all located events during Panel 2E development (times in GMT). ....	62
Figure 33: Inter-event distances for events with an average error of less than 100 ft. during Panel 2E development. ....	63
Figure 34: Magnitude distribution chart for all located events during Panel 2E development. ....	64
Figure 35: Future microseismic and borehole pressure cell monitoring. ....	71
Figure 36: BPC monitoring layout.....	72

## ***List of Tables***

Table 1: Event parameters of Trigger 266 on February, 26th 2015.....	49
--	----

# Chapter 1: Introduction

Ground control is a major issue in underground coal mines. The “soft” nature of the rock, nearby bedding, and seam depth are just a few of the factors that make coal extraction dangerous. In the United States between 2006 and 2012, over 3,300 injuries (fatal, non-fatal days lost, no days lost) were reported as a result of a fall of a roof or rib in the underground coal mine industry. This represents over 16% of all reported underground coal incidents during this period (MSHA, 2015). Forty-two of these injuries resulted in deaths. In comparison during this same time frame, underground metal mines had 13.5% (240 injuries) and underground nonmetal mines had 6.7% (55 injuries) of all injuries resulting from the fall of a roof or rib. Over the years, the number of injuries have decreased, but as of 2012 there were still 376 yearly injuries in underground coal mines across the United States (Figure 1).

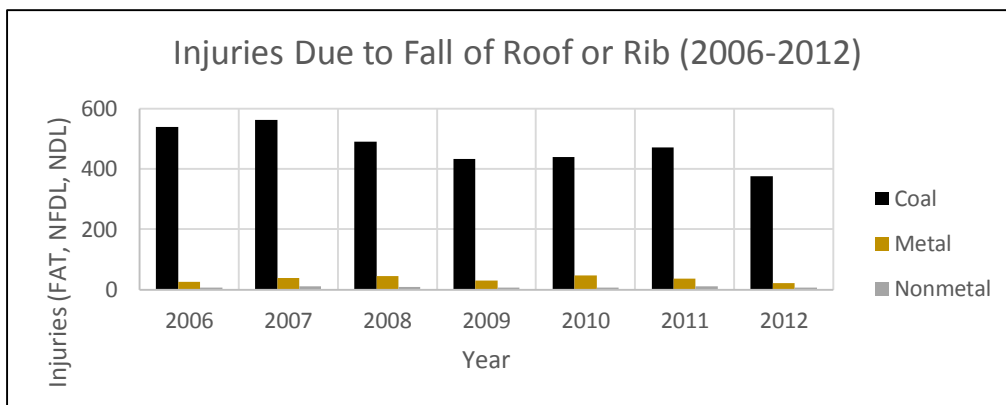


Figure 1: Injuries (FAT, NFDL, NDL) due to the fall of a roof or rib between 2006 and 2012 (MSHA, 2015).

Commonly accepted mining methods, such as longwall and room and pillar retreat, allow overburden to cave. This creates highly variable stress conditions that can be difficult to predict. From both the safety and production point of view, unplanned ground falls resulting from these conditions are unacceptable. Not only can fatalities and injuries occur, but falls can obstruct escape ways, block ventilation, cause stoppage in operations, damage equipment, and cause lost ore reserves. Proper mine design and safe operating procedures are critical to prevent ground control issues from happening.

A common way of determining instability and changing stress conditions in underground mines is to monitor mining-induced microseismic events. A microseismic event occurs when a rock under a critical amount of stress fractures and emits an energy wave of short duration and

small amplitude (Obert and Duvall, 1967). Each waveform contains a grouping of elementary wave signals that represent particle velocity initiated by individual pulses of stress wave energy (Descour & Miller, 1987). The energy pulse's shape details the amount of stress released at the source and the effect of non-uniformities in the rockmass along its travel from the source to a microseismic sensor such as a geophone. The polarity of a waveform from both manmade and natural sources can be used to determine whether an event's driving force was shear or compressional (Swanson et al., 2008). Individual waveforms are analyzed to determine the time, location, and magnitude of a single event. A seismic event with a moment magnitude of typically less than 2.0 is considered "micro" (Spence et al., 1989). Over time, the failure process of a monitored area can be studied from the progression of the located events.

At least three microseismic surveys have been completed and analyzed in longwall coal mines (Luo et al., 1998; Ellenberger et al., 2001; Luxbacher et al., 2007; Swanson et al., 2008; Alber et al., 2009). These studies and analyses verified that microseismic monitoring is a useful tool for understanding stress redistribution in an underground coal mine setting. In contrast, room and pillar retreat mines have had only one published microseismic study. This study, completed in 1987 by Descour and Miller, monitored various parts of a retreat mine section over a 10 month period. The mine layout however was not the same as what is currently found underground. Modern rectangular retreat panels, which incorporate five to seven entries encompassed by barrier pillars on both sides, were not employed. Instead, an entire section of the mine was extracted. Much smaller barrier pillars, approximately the size of 10 production pillars, were placed in vital areas of the section.

This research involves the microseismic monitoring of a room and pillar retreat coal mine panel throughout the retreat process, as well as approximately two months of development for the next panel in the section. The mine site was located within the Jawbone coal seam in southwest Virginia. Retreat data was collected for approximately 1.5 months with the use of eight geophones in the mine roof. Six geophones were located along the first entry of the panel and two were placed in the mains. Events were located and their moment magnitudes were found. The magnitudes and locations of the events were compared to the mine geometry and face location to determine where higher amounts of stress were located.

## **Chapter 2: Literature Review**

### **2.1 Room and Pillar Retreat Mining**

#### **2.1.1 Description**

Room and pillar retreat mining, otherwise known simply as “retreat mining,” is a popular method of extracting coal from relatively flat underground reserves. Retreat mining is used instead of other popular underground coal extraction methods such as longwall mining because of capital equipment costs and simplicity (CSM, n.d.).

During the mining process, rooms are driven in a coal seam using continuous miners and a haulage system of either shuttle cars or conveyor belts directly from the miner. A checkerboard pattern is created which leaves large blocks of coal (pillars) in place to support overburden and prevent collapse. The pillars of coal that were left during development are then removed (pulled) in the opposite direction on retreat to maximize the recovery of the coal seam, leaving overburden to cave behind the active mining face. Pillar recovery accounts for approximately one-third of production time in a typical retreat mine (Mark et al., 2003). Usually around 60% of the coal is extracted (CSM, n.d.). Recovery must be maximized to ensure that coal is not lost to fairly compensate the landowner for their property. In the case of mining on public lands, permit approval is partially based on whether the site achieves maximum economic recovery, as determined by the US Department of Interior’s Bureau of Land Management (BLM) (NIOSH, 2010). Typically, retreat mines are limited to shallower depths because larger pillars are needed deeper underground to control ground issues, thus reducing extraction ratios.

The retreat process has been historically proven to be less safe than other underground coal extraction methods, accounting for 25% of all roof and rib fatalities with 10% of underground coal production in the 10 years between 1986 to 1996 (Mark et al., 2003). It was found in the 2003 study that retreat mining heightens the chance of a miner being killed in a roof fall by a factor of three. Safety in retreat mines has though improved. Through the increase use of roof support, new technology, and risk assessments, a four year period between 2007 and 2010 only had one fatal roof fall during retreat mining, compared with an average of two per year in the previous 10 years (NIOSH, 2010).

### **2.1.2 Deep Pillar Recovery**

Deep cover pillar recovery, in which U.S. legislation defines as having overburden in excess of 1,500 ft. (457 m.), continues to be an important issue as shallower seams are exhausted (Chase et al. 2002; Mark, 2009). The term “deep cover” also has been used by (Chase et al., 2002) and (Ghasemi et al., 2012) to describe pillar recovery over 750 ft. (229 m.) deep. Mine Safety and Health Administration (MSHA) statistics show that deep cover pillar recovery accounts for more than one-third of all underground coal roof and rib fall fatalities and injuries (Chase et al., 2002; Ghasemi et al., 2012).

Deep cover mines typically drive five to nine rooms (entries) to develop a panel (NIOSH, 2010). Barrier pillars are left between the panels to provide ground control support for abutment loads as well as for ventilation purposes. They act as a stress control to transfer loads to seams above and below, and separate active panels from the stresses of adjacent panels, otherwise known as abutment loads (Chase et al., 2002). Some mines drive rooms into the barrier pillar to achieve a higher coal recovery. The deeper a retreat mine is, the more important barrier pillars become to reduce stress on the active panel. It is recommended by Campoli et al. that barrier pillars are not needed with less than 1,000 ft. (305 m.) of cover, but should be used for deeper depths, with barrier pillar sizes ranging from 150 to 240 ft. (46 to 73 m.) in up to 2,200 ft. (670 m.) of cover. The width of a barrier pillar depends on the stress rise over an abutment as well as the total weight of the overburden (Yavuz, 2004). Mark (2009) stated that mines that encounter multi-pillar bumps usually have barrier pillars too small or are extracted on retreat.

### **2.1.3 Retreat Mine Loading**

When a retreat panel is developed, a portion of the coalbed is left to create pillars to support the weight of the overburden. Once created, the roof-pillar-floor system wants to close the opening between them. Stress concentrations, known as the tributary loads, arise. These loads are determined by the thickness of the overburden and the extraction ratio. If the pillar is adequately sized, whereas there is enough roof contact to support the load and adequate floor contact to hold the load without failure, these concentrations will return to an equilibrium (Campoli et al., 1989). If loads become too great, deterioration in the form of perimeter yielding and sloughing will occur from a high load concentrated along the edge of the pillars. When this happens, the roof span is widened and an additional load is transferred to the competent coal.

The stress distribution in the pillar is controlled by the physical properties of the roof, floor, coalbed, and pillar geometry. Generally, stresses are low near the pillar edges and rapidly increase towards their center. The state of stress though is dependent on the pillar's width and length of time it has been supporting the load. If a pillar is wide enough, the stress level in its center is much lower than near its edges (Campoli et al., 1989).

As pillars are recovered during retreat, an unstable rock mass is created in the pillar line causing the roof over the retreated area to be subjected to greater stress and deformation (Mark et al., 2002). Once this area hits a critical point, overburden begins to cave into void left from extraction in an incremental fashion closely matching the daily extraction rate. Failure is highly dependent on the rate of extraction, with higher rates corresponding with higher mining progress (Iannacchione et al., 2005). The failures that create the gob eventually propagate to the surface, creating subsidence effects.

Abutment loads are created from the transfer of stresses created in adjacent in-situ coal. These loads act commonly to narrow pillar yielding, where a stress arch is created due to the pillar's inability to carry further loads (Mark, 2009). The previously carried loads then get transferred to surrounding areas of solid coal, resulting in roof-to-floor convergence of the entries. While retreating, the stress distribution within the gob area is tough to quantify. The effect of the abutment zone forces however can be seen on the active pillar sections by convergence outby the pillar line, which represents the entire movement of the roof-pillar-floor structure (Campoli et al., 1987). Figure 2 displays the development and abutment loading that is applied to the active pillar sections. Effects of the additional front abutment loading occur in the active mining zone (AMZ) from 10s to 100s of feet inby the pillar line, depending on the depth of cover, adjacent strata, and the physical properties of the coal bed.

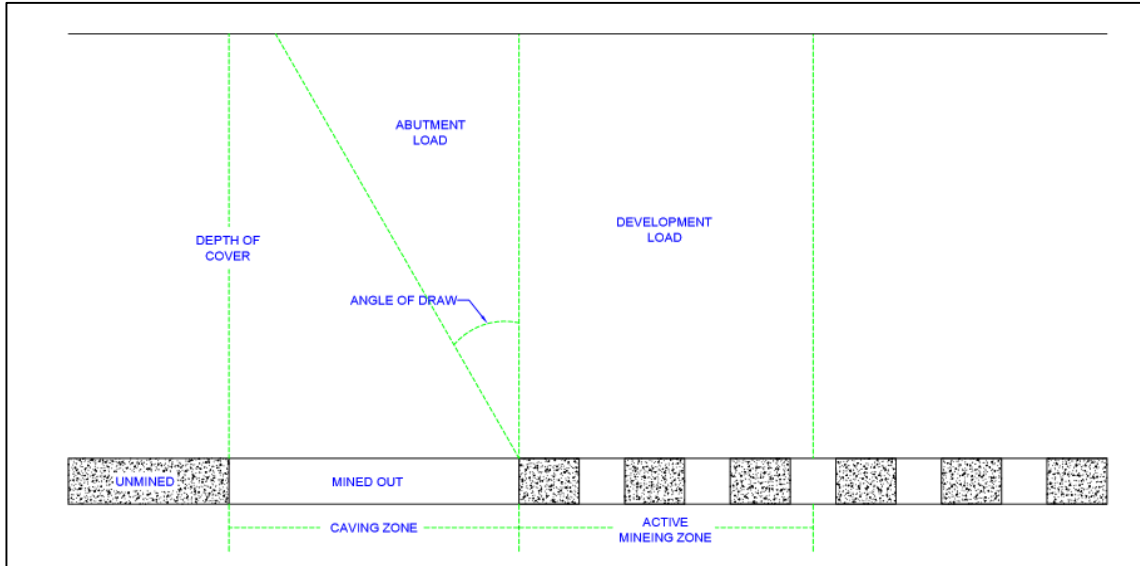


Figure 2: Loadings applied to a retreat panel (after ARMPS, 2013).

The AMZ is the area that receives additional loading from the retreat process. This area receives both tributary area loads from development, as well as abutment loads that form on the side and front of the mined out gob area. Ninety percent of front abutment loads occur in the AMZ, which extends across the entire pillar line and a distance outby of five times the square root of the depth of cover (Mark, 1990). Abutment stresses are greatest near the gob and decay as the square root of the distance outby the gob edge. The width of the AMZ is taken as the distance between all center-to-center spacings within a panel.

The magnitude of loading on any unmined coal (abutment) nearest the gob area is determined by a portion of the total volume of gob overburden. This portion is dictated by the abutment angle of the load, which is generally considered to be approximately 21 degrees (Figure 2) (ARMPS, 2013). Figure 3 details the extent of the abutment load applied on the active mining zone. Past field measurements have indicated that the range of the abutment zone (D) at depth (H) is approximately:

$$D = 9.3\sqrt{H}$$

and that 90% of the abutment load should be located within (Mark, 1990):

$$D_{0.9} = 5\sqrt{H}$$

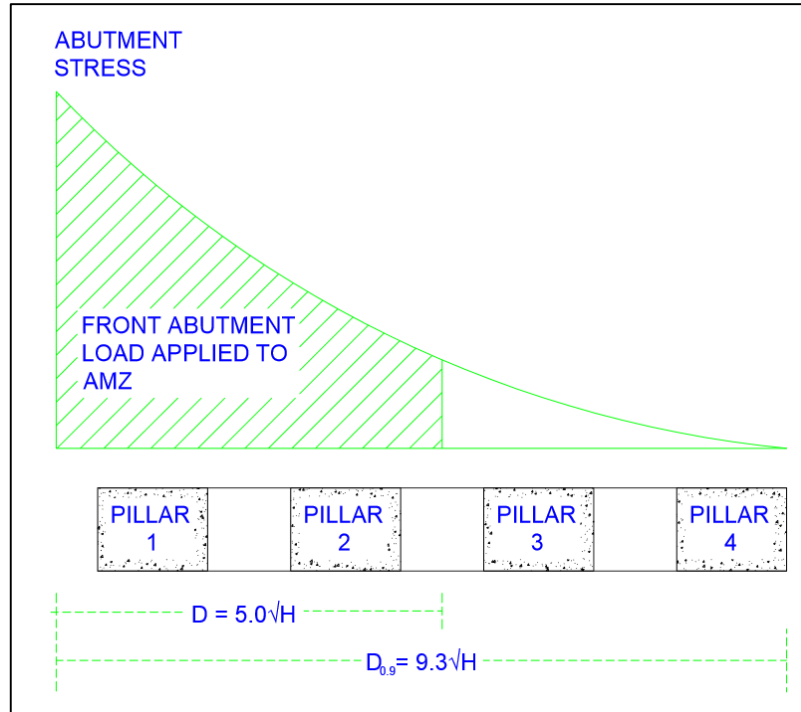


Figure 3: Abutment load distribution to the active mining zone (after Mark, 1990).  $D$  is the extent of the abutment zone while  $H$  is the depth of cover.

Barrier pillars are designed to carry a portion of the front abutment load as well as the pillars destined for recovery. Some of the abutment load will be transferred back to the AMZ if barrier pillars are too small. If some of the load from retreating is distributed to pillars outby the AMZ, the front abutment load is reduced. Side abutment loads from previous panels are shared between the barrier pillars and the AMZ. Just like with front abutment loads, the abutment angle and gob extent determine how large of a load occurs. The total amount shared to the AMZ depends on the width of the barrier pillar.

### 2.1.4 Pressure Arch Theory

A pressure arch is created when barrier pillars are applied to a retreat panel. The overburden load is transferred by the stiff roof over the panel to adjacent barrier pillars. As a result, remnant pillars are isolated from the entire overburden load and receive a reduced amount of stress compared to a layout of no barrier pillars (Mark & Tuchman, 1997). Abutment stresses can be reduced to pre-mining levels at a certain distance within the excavated panel. Figure 4 shows the ARMPS loading model for a pressure arch with side gob and an adequate barrier pillar. In all, the redistribution of in situ stress depends on the overall extraction ratio and a

barrier pillar's zone of influence (Poulsen, 2010). Pressure arches do have the possibility to break down if the panel between successive barrier pillars is too large to support the roof's bridging capacity, faults are present, or if the roof or remnant pillars weaken over time. If a breakdown occurs, the full amount of overburden load is transferred back to the remnant pillars and a CPF can occur (Mark & Tuchman, 1997).

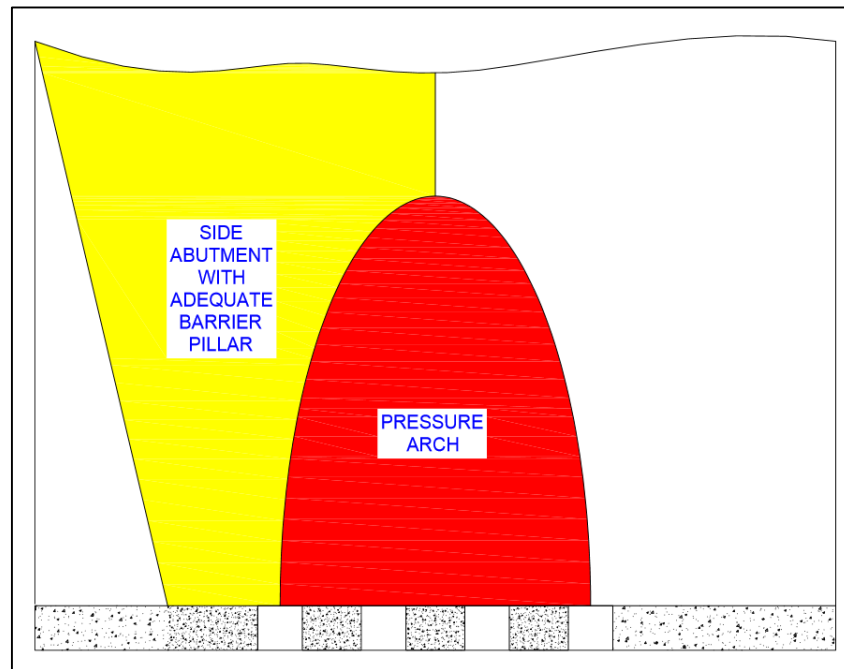


Figure 4: Typical retreat panel loading model with barrier pillars and pressure arch (after ARMPS, 2013).

### 2.1.5 Subsidence

Subsidence is unavoidable while retreat mining and can cause issues to structures on the surface. During retreat, stratum in the overburden are disturbed the greatest in the immediate roof and least towards the surface due to caving. The immediate roof caves behind standing supports to fill the void left from the retreat process. This void is equal to the cut height of the extraction. The compacting characteristics of the roof determine the magnitude it will lower to the floor. Upper strata then collapse on the immediate roof in a way relative to their thickness, properties, type, and nature (Yavuz, 2004). Over time, the caving process propagates to the surface, producing a subsidence area above the retreated panel. Subsidence may occur immediately after retreating and continue after mining has ceased. Figure 5 displays the front profile of a retreated

panel with horizontal movement, tensile and compressive strain, the angle of draw, and typical subsidence profile labeled.

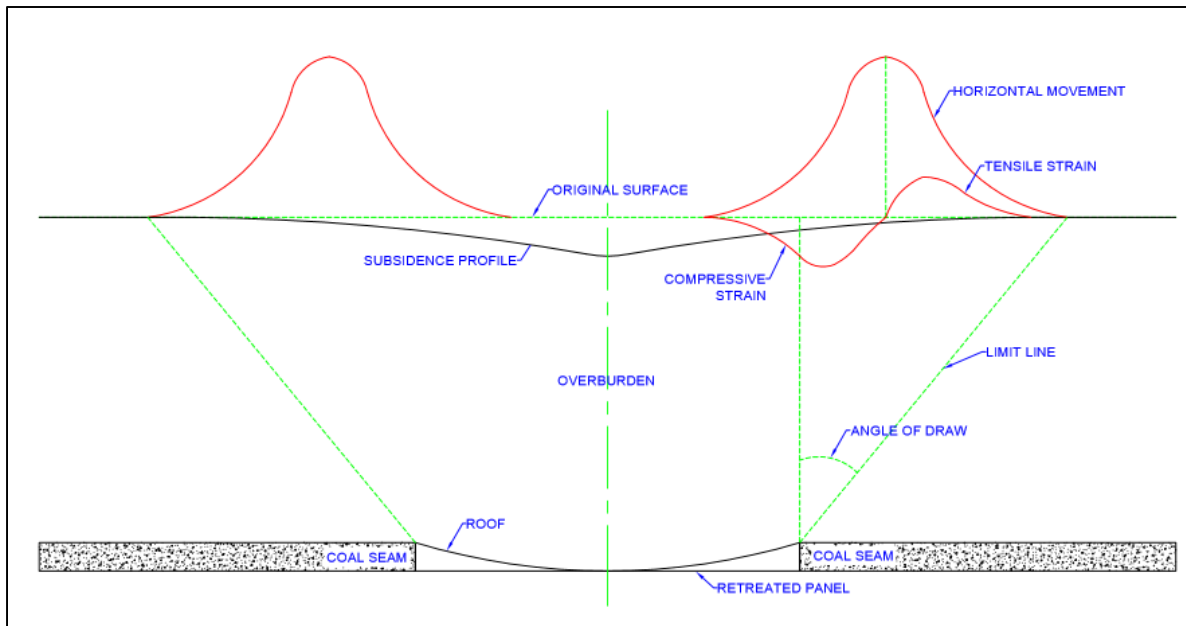


Figure 5: Mining subsidence profile (after Ren & Li, 2008).

It has been found that the subsided area is larger than the mined out area, having an angle of draw usually between 25 to 40 degrees from the boundaries of a retreated panel (Ren & Li, 2008). Angles of draw are dependent on the depth of cover and seam angle, as well as the strength and composition of the overburden strata. Stiffer strata are able to reduce the amount of subsidence as well as the angle of draw. The maximum amount of subsidence that can be observed is equal to the cut height of the mine, but actual movement occurs on a scale of centimeters or inches. “Bridging effects” where pressure arches are formed over the panels can also significantly reduce subsidence.

## 2.1.6 Design Parameters

### 2.1.6.1 Global Stability

Two types of stability are needed to adequately provide safe working conditions underground: global and local (Mark et al., 2002). Global stability is accomplished by properly designing a mine, primarily its pillars. Pillars carry the weight of the overburden, up to thousands of feet thick, and must be able to maintain support without failing through squeezes, massive

collapses (cascading pillar failure), and bumps. Under deeper cover, the chance of pillar failure increases.

Pillar squeezes, the most common type of pillar failure, occur when pillars are undersized for the loads they must carry (NIOSH, 2010). They are the most likely failure mode when overburden is less than 1,250 ft. (381 m.) (Chase et al., 2002). When loads are transferred due to mining, adjacent pillars tend to fail, resulting in the severe rib spalling, roof failure, floor heave, and the ultimate closure of entries (Mark et al., 2002). The process can take only a few hours or days. Squeezes are not violent events and occur more slowly than other failures such as bumps. Less injuries to workers are of a result of these events because affected areas can be identified and abandoned before becoming too dangerous (NIOSH, 2010).

Massive collapses, otherwise known as cascading pillar failure (CPF), progressive pillar failure, domino-type failure, or pillar run, are when one pillar becomes overloaded and collapses, resulting in a rapid transfer of load to adjacent pillars, causing those to subsequently collapse (Zipf, 2001). Pillars will continue to collapse until loads have settled and they encounter a strong supporting rock mass. As a result of a massive collapse, a few tens or up to hundreds or thousands of pillars may fail (Zipf, 2001). Damage can appear similar to other failures such as bumps and rockbursts.

Mines with certain types of characteristics are at more risk for a CPF. Those include extraction ratios of greater than 60%, width-to-height pillar ratios less than 3, panels more than 5 pillars wide, and no barrier pillars with a width-to-height ratio greater than 10 (Zipf, 2001).

The mechanics of a massive collapse “depend on the applied vertical stress and the post-failure, strain-softening behavior of the pillars” (Zipf, 2001). Post-failure stiffness and the remnant pillar strength are the most important structural characteristics of a collapse. Stiff and massive roof rock can also increase the chances of massive pillar collapse by creating wide bridge spans that inhibit caving and load reduction.

After the pillars rapidly reduce their load and fail, they are left with very little strength. Slender pillars with low width-to-height ratios display this trend, while those that are squatter will more likely squeeze because they retain most of their load. Of all of the massive collapses occurring in the United States, the pillar width-to-height ratio was 3.0 or less, pillars had a safety factor of less than 1.5, and barrier pillars with width-to-height ratios of greater than 10 were not present (Mark et al., 2002; Zipf, 2001). These situations occur most often when pillars are split to

increase recovery (Mark et al., 2002). At a width-to-height ratio of about 3 to 4, post-failure behavior changes from strain softening to elastic-plastic deformation. A massive failure at this point becomes impossible because this is where conditions change from rapid failure to a slow, nonviolent manner (Zipf, 2001).

Ground issues are not the only dangers from massive collapses. Due to the rapid displacement of air from pillar failures, an air blast can be created. An air blast can cause injury or death to miners by flying debris or being thrown against a rib. It can also be extremely damaging to ventilation controls such as stoppings and seals (Zipf, 2001). The fracturing of large amounts of coal might release a large volume of methane gas into a mine's atmosphere as well, creating the risk of explosion.

Coal pillar bursts, also called pillar bumps and outbursts, are when high stresses in a pillar cause it to rupture without warning (Mark et al., 2002). They share characteristics of both bursts in hard rock mines and seismic events (Mark et al., 2003). It is important to note that while bursts are seismic events, not all seismic events are bursts. Coal bursts are created by the change of loads due from removing the coal that is confining the most highly stressed pillar (Mark, 2009). The damage can affect a small part of one pillar or destroy many pillars at once (Zipf, 2001; NIOSH, 2010). Hard to predict sandstone channels, multiple seam interactions, and pre-existing faults generally lead to a higher risk of a burst (Mark, 2009). Coal seam characteristics do not appear to be significant in creating bumps. They have occurred in coalbeds that are strong and blocky as well as those that are very friable. Unconfined compressive strengths in these coalbeds have ranged from 700 to 7,000 psi (Mark, 2009). Pillar design can greatly reduce the chance of a burst, but there are many other causes that affect their occurrence. Bursts are also much less likely when barrier pillars are employed to isolate the abutment loads coming from previously mined gob areas. In all, retreat mining has accounted for 50% of all bumps occurring in the United States, and 95% have occurred at depths greater than 1,000 ft. (305 m.) (Mark et al., 2002).

#### Crandall Canyon

On August 6<sup>th</sup>, 2007 six miners lost their life at the Crandall Canyon mine near Price, Utah (Mark, 2009; MSHA, 2007). A violent, large scale coal outburst trapped the miners in a

retreat mining section with a cover of 2,200 ft. (670 m.) at its deepest point. While rescuers were searching for the miners' location, a second bump occurred 10 days later, killing three others.

The Mine Safety and Health Administration (MSHA) concluded that the incident was caused by a "flawed mine design" due to the stress level of a single pillar or group of pillars being exceeded (MSHA, 2007). The local failure began a widespread collapse (CPF) throughout the section of similarly sized pillars. It was found that empirical and numerical models were improperly applied by the operator and consultant company. From this disaster, the U.S. Congress tasked governmental agencies in determining safer deep cover pillar extraction.

### ***2.1.6.2 Pillar Design***

To create a pillar design, there are three basic steps that must be taken (NIOSH, 2010). First, an estimation of the applied loads, including abutment loads must be completed. In addition to the loading, the strength of the coal pillars must be determined. Finally, a comparison between the load and strength to determine a safety factor will show whether the design is adequate. To accomplish these steps, two different methodologies are employed. Empirical methods use historical data to estimate pillar strengths and loads, such as the Analysis of Retreat Mine Pillar Stability (ARMPS) program. Numerical methods attempt to reproduce rockmass behavior through computational modeling. LaModel is a popular numerical modeling tool used in retreat mining.

#### ***2.1.6.2.1 ARMPS***

Analysis of Retreat Mining Pillar Stability (ARMPS) is an empirical modeling software developed by the National Institute of Safety and Health (NIOSH) that is used to design pillar sizes for retreat room and pillar retreat mining. The software calculates stability factors that are based on an estimate of the strength of the designed pillars and the expected loads they will experience during various stages of the retreat mining process. ARMPS uses both tributary (development) and front abutment loads during calculations (ARMPS, 2013). It also takes into account crosscuts, various entry widths, bleeder pillars, gob areas, and barrier pillars. ARMPS employs a vast database of more than 600 field studies that were back-analyzed to calibrate the software. As a rule, when the depth of cover for a design is less than 650 ft. (198 m.), a stability factor of 1.5 is a justifiable condition. Under more cover, a "pressure arch" can form above the panel that places a higher load on barrier pillars and reduces the load on the production pillars.

The default pressure arch factor in ARMPS is set to 0.74. Because of the pressure arch phenomenon, a stability factor of 1.5 is adequate under deeper cover as well. Barrier pillars are recommended if retreating at a depth of cover greater than 1,000 ft. (305 m.). Their stability factor should be greater than two (ARMPS, 2013).

An important aspect in determining the stability factor of the designed pillar system is the active mining zone (AMZ). This zone includes all of the pillars that receive higher loads due to the retreat process. All pillars on the pillar line (“extraction front”) and those that extend outby the line, a length of five times the square root of the depth of cover are accounted for. The stability factor is taken for the entire AMZ since the pillars within the zone have shown to usually perform as a system. If a single pillar is overloaded, the excess load will typically transfer to neighboring pillars. If those pillars are appropriately sized, load transfer halts, but if they fail a domino effect can take place with possibly a massive collapse (ARMPS, 2013).

#### ***2.1.6.2.2 LaModel***

A common numerical modeling tool for pillar design is LaModel. The software is a boundary element, “displacement discontinuity” program that estimates stress displacements of thin tabular deposits (NIOSH, 2010). Laminations are used to model layered, sedimentary overburden. Outputs are a three-dimensional analysis of large coal mine areas. Advantages of the software over empirical methods such as ARMPS include being able to input complicated geometries, use strain-softening seam materials, and account for multiple seam interactions and varying topography (NIOSH, 2010).

Just like any numerical software though, results are highly dependent on the material properties and other input parameters. Regular observations are needed to confirm a model’s accuracy (NIOSH, 2010). Because exact measurements are most likely not known throughout the analyzed area, LaModel is paired with empirical modeling software such as ARMPS. Researchers have also established procedures for calibrating LaModel to begin with a baseline model that corresponds with ARMPS and its broad database (NIOSH, 2010). More intricate models can then be created to cater to the design needs.

### **2.1.6.3 Local Stability**

Ensuring global stability in an underground coal mine cannot solely create a safe working atmosphere. Local stability is also needed to ensure ground control is adequate. Cut sequence, final stumps, mobile roof supports, and roof bolting all affect the stability of a mine. Other risk factors that influence local stability include roof geology, intersection span, depth of cover, multiple seam interactions, recovery of old pillars, non-uniform pillar dimensions. Miners are at risk only if failure occurs prematurely, as remaining pillars and supplemental support should reinforce the overburden inby (Mark et al., 2002).

#### **2.1.6.3.1 Cut Sequences**

The most common cut sequence is the “Christmas tree” pattern, also known as “left-right” (Mark et al., 2002; NIOSH, 2010). It is almost universally used for pillar recovery in Central Appalachia. The Christmas tree method takes cuts from both the left and right pillars. Risks include wider unsupported spans, more time spent in one location, and the operator position, which is not at an optimum area. The method can however be safer extracting wide pillars. It also does not create an extremely deep cut, which allows for an easier removal of man or machine if entrapped by a ground fall.

The second most popular cut sequence is the outside lift. This method only mines one pillar at a time, taking only lifts from the left or right. Advantages include having shorter roof spans than the Christmas tree method and not being located in a single area too long. It is not ideal though for large pillars that are sometimes required for global stability. It also creates deeper cuts than the Christmas tree method, possibly generating a more difficult extraction in the event of a ground fall (Mark et al., 2002).

Other cut sequences include “split and wing” and “pocket and finder” which both require splitting pillars before full extraction. In these cases, supplemental roof bolting is mandatory, creating more operating costs. Splitting techniques create a higher chance of burst since the highly stressed core of the pillar is initially removed, quickly placing the pillar’s load on its resulting remnants (NIOSH, 2010).

#### **2.1.6.3.2 Final Stump**

The final stump, otherwise referred to as a “pushout,” is the last remaining part of a coal pillar left when retreating to provide support to unstable intersections. This area is weak because

of its wide span. Historically, the pushout has been removed in retreat mines for fear that it would inhibit caving and cause a squeeze, even though over half of the fatalities during retreat involved the last lift. This idea has been disproven by recent experience and in the last decade many retreat mines are leaving the final stump for support (Mark et al., 2002).

#### **2.1.6.3.3 Mobile Roof Support**

Mobile Roof Supports (MRSs) have largely replaced timber posts as supplemental support at the pillar line for full recovery. Setting timbers is a risky task that requires labor to handle heavy pieces of wood under unstable roof. More than 100 posts may be needed to remove a single pillar. A miner setting timbers is twice as likely to be injured as one operating an MRS. As of 2010, only around 15% of 30 studied retreat mines didn't use MRSs. These pieces of equipment can be set remotely and can maintain their load even under more than a foot of convergence. Their only disadvantage is that they are expensive which makes recovery necessary if they get entrapped in a ground fall. Pairs of MRSs are needed to be able to support each other as they move (Mark et al., 2002; NIOSH, 2010).

#### **2.1.6.4 Major Parameters Contributing to Ground Control Issues**

##### **2.1.6.4.1 Depth of Cover**

As retreat mines progress deeper into the earth, higher levels of stress, both vertical and horizontal, are encountered. More ground stability issues arise as a result, creating a need for additional support to ensure safety. To help with this issue, properly designed barrier pillars should be left to isolate the stress surrounding active panels. Horizontal stress relieving techniques may be used to improve mining conditions. Cut sequences should also be appropriately selected to improve mining conditions.

Support is also a concern for shallower mines. For retreat mines less than 40 meters deep stress is less of a concern, but due to surface effects overburden can be brittle and unpredictably fail (Ghasemi et al., 2012). Extra support and the appropriate design of smaller entries is needed to safely excavate the coal.

##### **2.1.6.4.2 Roof Rock Quality**

The quality of roof rock in retreat mines is important to note for safety. The strength of the rock, moisture sensitivity, bedding planes, and other discontinuities must be known to

determine if higher levels of roof bolting and shorter roof spans are needed. Abutment loads have been found to affect weaker roofs more than stronger roofs (Ghasemi et al., 2012). In retreat mines, overlying massive strata must be considered as much as weak strata. To prevent air blasts and protect the pillar line, roof collapse should occur uniformly and at a constant, proper distance. Strong, overlying strata can ‘hang up’ and cause extra stress on the pillars, creating a higher likelihood of bursts (Ghasemi et al., 2012). These large sections of roof that have yet to cave can reach a critical span length and fall at once, resulting in an air blast that is unsafe for miners and equipment.

A tool to help bridge the gap between geologic characterization in coal bedding and engineering design is the Coal Mine Roof Rating (CMRR). The CMRR, created by (Mark & Molinda, 2007), uses a rating system between 0 to 100, where 0 indicates the very weak roof and 100 signifies extremely strong roof. The risk of roof fall is extreme when the CMRR is less than 45, high between 45 and 55, moderate between 55 and 65, low between 65 and 85, and negligible greater than 85. The lowest CMRR Mark & Molinda (2007) measured was 45, but most mines had a typical CMRRs value in the 50s. Only a few mines had “strong” roofs with a CMRR greater than 60. These did not report any problems with roof caving due to massive sandstone formations (NIOSH, 2010).

Bedding has historically been the largest cause of roof problems in coal mines (Mark & Molinda, 2007). Weak laminations in shales and thinly interbedded shale and sandstone commonly cause ground control issues in coal mines as these structures frequently form above coal beds. In the case of retreat mining, strong bedding can be an additional issue. Rock failure may not occur at the face due to the stress and deformation gradient being reduced compared to the continuous incremental failure (Iannacchione et al., 2005). As a result, strong structures, such as those with a sandstone composition, can be suspended over a large area and inhibit caving. Once a critical stress for the area is reached, the roof can violently fail over a wide area. Events can be very large and not correspond closely with the mining rate.

Moisture sensitivity of the roof rocks is also a concern. If a rock type is susceptible to disintegrating when exposed to groundwater, the strength of the rock in the roof will be reduced. This can create swelling pressures or cause sloughing, making roof support ineffective (Mark & Molinda, 2007). Another important factor in the roof rating is the presence of discontinuities. Discontinuities such as slickensides often occur in addition to bedding and create unstable roof.

Large-scale features, which include sandstone channels, faults, veins, and seam rolls are not directly included in the CMRR. These structures should each have their own CMRR with concurrent designed support systems (Mark & Molinda, 2007).

#### ***2.1.6.4.3 Floor Quality***

In general, floor rocks tend to be more firm and considerably stronger in the retreat mining areas of Colorado, Utah, and Central Appalachia than in the other U.S. coalfields (NIOSH, 2010). Floor quality is an important parameter in the safety and operation of retreat mines since floor rock provides the foundation of support for the pillars and roof. All three sections of an underground mine should be looked at as a complete system, where each depends on another. For example, if competent roof is present, overstressed pillars can punch into a weak floor and cause heaving in the entries. This can lead to impassible roadways, dangerous pillar spalling, and roof convergence and failure (Chase et al., 2002; Ghasemi et al., 2012). Mine designs should properly design panel, pillar, and entry dimensions to account for weak floor.

#### ***2.1.6.4.4 Groundwater***

Retreat mining creates joints and fractures in the overburden when caving occurs, possibly allowing water in upper strata to flow into the mine and cause further instability near the pillar line (Chase et al., 2002; Ghasemi et al., 2012). Groundwater is rarely a problem though in U.S. coal mines greater than 1,000 ft. deep (305 m.) (NIOSH, 2010). The hazard of rock fall depends visually on the amount of water coming from the roof. When no water can be seen, falls resulting from groundwater are not probable. The probability of roof fall is low if the roof is damp. As the roof becomes wetter and there becomes a constant inflow of water, roof fall is much more likely (Chase et al., 2002; Ghasemi et al., 2012).

#### ***2.1.6.4.5 Multiple-Seam Interaction***

Coal seams typically form close to each other in geologic time, separated by varying amounts of rock strata. As more economic reserves diminish, mining companies are left with extracting seams above and/or below previously mined areas. Approximately 80% of all deep cover retreat mines have workings less than 200 vertical feet from active seams (NIOSH, 2010). Interactions between mined out seams can cause roof falls, pillar failures, floor heave, and bursts if not adequately accounted for in design plans (Ghasemi et al., 2012; Mark & Molinda, 2007).

Interburden distance, the distance between two coal seams, is the single most important factor when determining the amount of interaction (Ghasemi et al., 2012). Other factors that affect seam interaction is the depth of cover, interburden geology, mining direction, and the remanent structure of previously-worked areas. To mitigate these risks, mines can install extra roof support, develop longer pillars, create narrower entries, or completely avoid the area (Ghasemi et al., 2012). Unlike geologic features such as sandstone channels, previously worked-out mines can often be identified before new development.

To aid mine designers in evaluating the risks of multiple seam interactions and mitigating them, NIOSH developed an empirical design method called Analysis of Multiple Seam Stability (AMSS, 2013; NIOSH, 2010). More than 300 case studies from 40 mines were analyzed with logistic regression, a multivariate statistical technique (NIOSH, 2010). AMSS evaluates pillar designs by calculating a stability factor with a single seam, and then computes a simple numerical model that adds additional multiple seam stress. If the stability factor is not adequate, pillar widths can be increased, crosscuts can be removed, or entry width can be reduced for a safer design (NIOSH, 2010). LaModel, as previously discussed can also aid in the assessment of multiple-seam interaction.

## ***2.2 Microseismic Monitoring***

### ***2.2.1 Purpose***

A passive microseismic event is a subaudible seismic event that occurs when a rock under a critical amount of stress fractures and emits an energy wave of short duration and small amplitude (Obert and Duvall, 1967). An event typically has a local magnitude less than 2.0 (Spence et al., 1989). The failure process of a monitored area can be studied over time from the waveforms of events. Each waveform contains a grouping of elementary wave signals that represent particle velocity initiated by individual pulses of stress wave energy (Descour & Miller, 1987). The energy pulse's shape details the amount of stress released at the source and the effect of non-uniformities in the rockmass along its travel from the source to a sensor. The type of driving force for the source, whether manmade or natural, is also given off from the event.

Microseismic monitoring has been used in a variety of underground conditions. Historically, the process has been largely employed in the oil and gas industry to monitor

hydraulic fracturing. In the mining industry, microseismic monitoring has been used for detecting rock failure, defining surface subsidence, finding in situ elastic properties of rock, and determining the distribution of stress instability within a rockmass. Seismic events are created by the detonation of small blasts, or by the fracture or movement of rock (Obert & Duvall, 1967). Typically monitoring has been performed on longwall panels in underground coal mines, but all types of underground mines, from hard rock to soft rock, have employed microseismic systems to monitor for ground stability (Gale et al., 2001). Obtained information has been paired with in-situ instrumentation (extensometers, stress cells, etc.) and numerical monitoring to explain rockmass behaviors. Stress zones of joint systems, as well as abutment zone boundaries are also able to be found from the concentration of microseismic events (Descour & Miller, 1987). Whenever rock is extracted underground, the support holding the overhead rock is removed, causing stresses to shift and build up around the opening. Thus, mining is the main source of instability with resultant microseismic activity (Descour & Miller, 1987).

### **2.2.2 Rock Failure Modes**

Rockmasses in-situ may have failure in five different modes (Gale et al., 2001):

1. Shear fracture through intact rock
2. Tensile fracture through intact rock
3. Shear fracture of bedding planes
4. Tensile fracture of bedding
5. Movement of pre-existing fractures

Each of these failures in conjunction with the size of their fracture result in a different stress modification. When a failure occurs, the immediate stress in the fracture is reduced from that of the intact material to a stress dictated by the strength properties of the actual fracture. The difference between these two amounts of stress is commonly referred to as the “stress drop” (Gale et al., 2001). Tensile failures provide stress drops of only 8-12% of the stress drops from shear failures. A shear fracture’s stress drop can be much greater from a compressive minimum stress than if the minimum stress was tensile. Shear and tensile failures for bedding planes will act in the same manner, but at different magnitudes than intact rock. Failures occurring on preexisting planes of weakness will only result in small stress drops from asperities or stick slip geometries (Gale et al., 2001).

As an effect of a stress drop of a fracture, stored strain energy is released. Just as with lower stress drops, tensile failures create much less energy than shear failures. The energy released is dependent on the strength parameters of the failing rock as well as the energy release per area of fracture (Gale et al., 2001). Strain energy released from a fracture can be calculated by:

$$\varepsilon = 0.5 * \Delta\sigma * \text{Area of Fracture} * \text{Displacement Across Fracture}$$

A simple depiction of shear and tensile failure in bedding planes is shown in Figure 6. Rock failure begins when the stiffest and thinnest bedding planes buckle from horizontal loading (Figure 6A) (Iannacchione et al., 2005). As a result, low-angle shears can occur through intact rock layers, while shear and tensile ruptures occur between the planes (Figure 6B). Additional low-angle shear failures are then created from lower confinement, causing roof beams to be strained to failure and cantilever. Over time, the cavity in the roof transforms into a more stable arch.

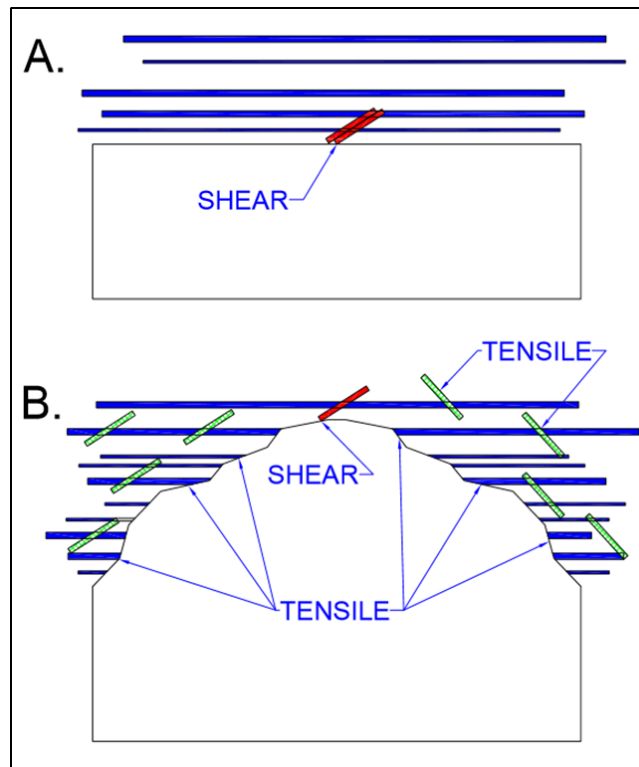


Figure 6: General progression of roof failure for high horizontal stress (after Iannacchione et al., 2005).

### **2.2.3 Formation of Microseismic Events**

Microseismic events are as a result of the sudden rupture and displacement of surfaces and their subsequent stress drop. Primary (P) waves, those that move in a compressional manner, and secondary (S) waves, those that move in a shear manner, are key factors in determining information about an event. The generation of these signals are due to the formation of fractures that propagate through the rockmass. The fracturing of the surface and subsequent network occurs at the velocity of the shear wave. When existing fractures are again mobilized, the failures release the amount of energy related with any asperities that previously caused the fracture to “lock-up” and any rapid movement along the preexisting fracture (Gale et al., 2001). In all, these slip events account for a small amount of the total energy released and can also occur without any detectable seismicity. This is also true with elastic deformation in the overburden, where much activity is too small to be seismically recorded, but can contribute to changing rockmass conditions that can cause failure.

Swanson et al. (2008) determined that waves from deeper natural seismic events appeared visually different than those produced by shallower mining events. Natural events begin with a sharp P-wave in the vertical direction, trailed by an abrupt S-wave in the horizontal direction. Mining-induced events appear with less distinguished P- and S-waves, with more phases and complexity that natural earthquakes do not exhibit. Also, these seismic events have a lower frequency but longer duration for same sized natural events. The differentiation between natural and mining-induced events is attributed to the mining-induced events remaining longer in the upper 1 km of the surface where there is a more “complex, rapidly varying, attenuating, low-velocity structure” (Swanson et al., 2008). Figure 7 displays the typical view of waveforms from naturally occurring and mining-induced events. The top three waveforms in the figure are from naturally occurring events, while the bottom three waveforms are from events that are mining induced.

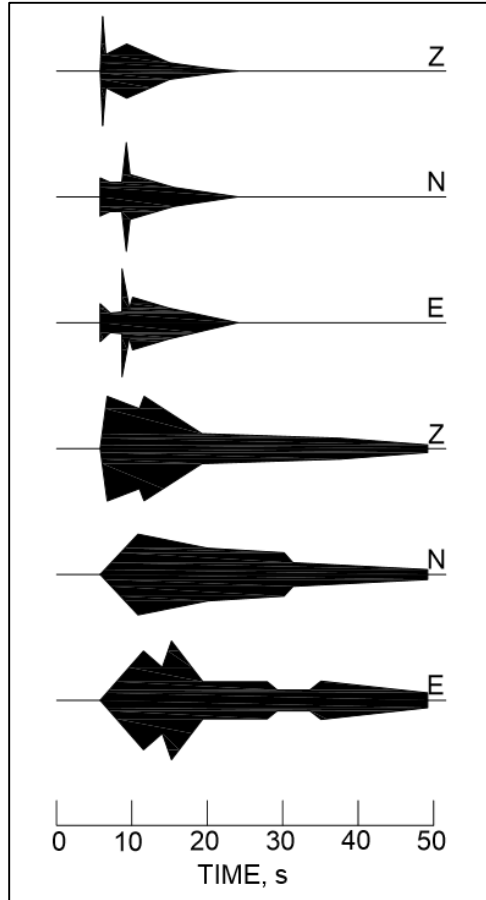


Figure 7: Typical waveforms from naturally occurring events (top three) and mining-induced (bottom three) events (after Swanson et al. 2008).

### 2.2.4 Moment Magnitude

To measure a rock failure's size, a moment magnitude calculation is used. The moment magnitude scale was developed by Hanks and Kanamori and is comparable with the Richter scale, commonly used to measure the size of larger natural earthquakes. The moment magnitude is expressed by the equation:

$$M = \frac{2}{3} \log(M_o) - 6.0$$

where  $M_o$  is the static seismic moment in N-m. This term is found by “the observed Fourier displacement amplitude spectrum of body waves, the rock density at the source, the body wave velocity, the body wave radiation pattern, and the distance between the seismic source and the receiver” (Iannacchione et al., 2005). The seismic moment also indicates the dynamic inelastic deformation of the seismic event.

### **2.2.5 Seismicity Relating to Ground Failure**

When a failure occurs, the resulting stress drop is propagated to the boundaries of the fracture. This process is largely dependent on the stiffness of the rockmass. When a system is “stiff”, where the “ground generating the stresses causing rock fracture (regional stiffness) is greater than the stiffness of the fractured rock zone,” individual fractures form in a stable mining atmosphere (Gale et al., 2001). These types of systems produce many low energy events. In the opposite case, a “soft” system, where the “regional ground stiffness is significantly less than the stiffness of the fractured rock,” failures occur rapidly in a large, unstable fracture network (Gale et al., 2001). Usually overburden movement assists in the loading with failures such as these. Soft systems produce single or high energy events from a lone fracture zone. As is the case in many instances, rockmasses are not solely stiff or soft, but are a moderate factor of each. Resulting events are usually a range of low to high energy occurrences.

### **2.2.6 Shear and Tensile Fracture Signatures**

Microseismic data can infer the nature of a failure occurring within a rockmass. The direction of the P-wave indicates whether shear or tensile failure occurred. A movement toward and away from the source (mixed polarity of up and down for vertical sensors) exhibit the features of a shear failure. When first P-wave motions move toward the source at all seismic sensors (first motion down with vertical sensors), the failure is tensile (Swanson et al., 2008).

Research has found that recorded seismic events typically occur in front of a panel’s face, within both the roof and floor (Gale et al., 2001; Heasley et al., 2001; Luxbacher et al., 2007). Strong P- and S- waves are recorded in these areas, with their polarization indicating that they were a result of shear failure. Shear events hundreds of meters away from sensors such as geophones were able to be picked-up (Gale et al., 2001). This is largely in part because shear events typically occur in highly stressed areas that allow propagation and absorb little signal.

Few tensile failures were recorded at the longwall sites. Tensile failure events are much more difficult be recorded by geophones because of their reduced energy. These types of failures occur where the seismic waves must propagate through highly fractured rock (gob) that has a high absorption. Tensile failure events are found to have approximately 10 times less of an amplitude than shear events. As a result, events needs to be within 150 ft. (46 m.) to be recorded by geophones. P-waves propagating from shear failure in the front abutment tend to be dominant

in the waveform, with their polarization signifying that the first motion of the failure was compressive.

### ***2.2.7 Wave Propagation Path Effects***

A waveform's character is strongly influenced by its propagation distance (Swanson et al., 2008). As waveforms travel through the rockmass, signals become elongated. The longer the distance between the source and receiver, the more paths of variable lengths waves can transmit. Each different path a waveform takes corresponds to a different travel time. An increase in distance traveled therefore increases signal duration. Since P- and S-waves travel at different velocities, the separation time between the waves also increase at longer distances. For example, even if a seismic event occurs adjacent to a receiver, signals will last significantly longer than those that reverberate within and between rock layers. In all, the duration of a signal is related to wave propagation path effects, and should not be corresponded to the length of the dynamic process that created the seismic waves (Swanson et al., 2008).

### ***2.2.8 Processing Levels***

There are three levels of processing in a microseismic system. The first level is receiving the transient microseismic waves that occur from structural failures in the rockmass. Each failure emits a wave that contains information about the type of failure and the stress conditions that it encounters on the way to a microseismic sensor (Descour & Miller, 1987). This wave travels through the rock and is picked up by geophones with known locations. If there no stress changes within the rock, the wave will propagate the same in all directions. The closest geophone will pick up the signal first, the next closest second, and so forth. The difference between the time it takes for the signal to reach the first and second geophone, second and third, and so on is measured. From these differences, it is possible to determine the point of failure (Obert & Duvall, 1967). If uniaxial geophones are to be installed, important to orient them towards the direction of interest so the sensor can more accurately respond to seismic P-waves coming from that area. The movement of the coil in a geophone is limited if seismic waves are transmitted at its side, as shown in Figure 8.

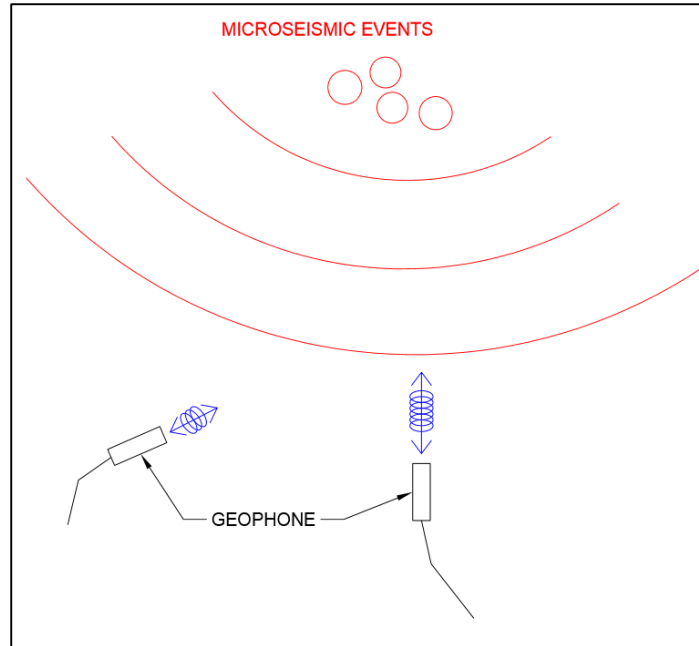


Figure 8: Impact of installation direction on a uniaxial geophone.

The second level of microseismic processing includes reconstructing the monitored rockmass's stress field in time and space from multiple failures. When a microseismic event occurs, it signals that the stress of a particular rock exceeded its strength, causing it to fail. Stress instability and rearrangement then occur simultaneously, which control the characteristics of a single microseismic event. The stability of a rockmass is in direct relation to the changes of stress in the existing system. In mining environments where larger openings are created, stress instability can build up and lead to violent ruptures such as outbursts or bumps (Descour & Miller, 1987). Past studies indicate that bump and roof ground control issues are caused by a non-uniform horizontal stress distribution occurring in the roof and floor.

The third and final level of processing is the most difficult. The goal is to predict where instability occurs, effectively controlling the rockmass while being mined. This is completed by a calibration to develop a model of failure and stress changes as extraction takes place (Descour & Miller, 1987).

### **2.2.9 Chain Reaction Failures**

Single failures in a rockmass are a result of growing instability within a multilevel stress envelope pyramid according to the chain reaction model (Descour & Miller, 1987). When an event occurs, the stress envelope of the area around the failure suddenly drops. This results in

surrounding stress envelopes receiving an increase in stress of equal proportion. The added loading is transmitted to the bottom of the stress pyramid inside each envelope. As more stress is incorporated, the rock's critical strength will be reached, causing further instability in the pyramid and thus another event. When rock is excavated near the bottom of the pyramid, as in mining practice, the result is a stress concentration and event occurrence. If an event occurs in a critical area, a chain reaction failure will occur over the entire stressed area until stress again becomes stable. The quickness of stress rearrangement in the system depends on the amount of loading on top of the overall pyramid (Descour & Miller, 1987).

### **2.2.10 Limitations**

Microseismic monitoring is not without its limitations. Because the rockmass at each monitoring site is different, monitoring must take place in real mine conditions and a simple encompassing model is not possible. Each failure is also difficult to precisely and accurately locate due to the ever-changing stress conditions. The location is the most important piece of information that can be recovered from a waveform. It indicates where the critical stress concentration point was reached and thus where the wave energy originated. It has been found that higher stress regions result in higher wave propagation velocity than lower stressed areas (Luxbacher et al., 2007).

Geology also plays a role in the non-uniform distribution of the velocity of the wave. Each layer in the rock mass has unique characteristics such as rock type and degree of fracturing/jointing that affect the how the wave travels from the source to sensors. Sensors near the source typically detect direct waves, but those further away from the source usually receive refracted waves. A velocity calibration can be performed by an event such as a blast, but is most likely not reliable unless the performed event is large enough to register throughout the whole area being examined.

Other limitations of microseismic monitoring include the sensor array. Due to costs and accessibility, a non-uniform system, not encompassing the complete monitoring area is usually installed. Under these conditions, the influence of anisotropy on a source's location is magnified (Descour & Miller, 1987). When a sensor array is within the transition zone between direct and refracted waves, this can be even truer. While not precisely known, these effects on the location of a source can be estimated from geologic and seismic properties of the rockmass.

Finally after microseismic recording, each level of processing is dependent on the previous level. If a poor sensor array is installed, sources will be hard to locate and stress changes will be difficult to determine. The model then created to predict instability related to stress conditions will be inaccurate.

### ***2.2.11 Microseismic Modeling***

Microseismic monitoring has been used in the past to confirm results gathered from numerical modeling. Failure zones in the models are typically compared to event locations. Reliability problems arise because geophysical data is not unique and up to 90% of damage and cracking in the rockmass is aseismic (Hazzard & Young, 2004). In order for models to be more dependable, they must be able to replicate both the failure of rock and associated induced seismicity with locations, magnitude, and failure mechanisms. This would allow the microseismic activity to be directly studied by accounting for site specific geophysical data and quantitatively comparing a model to actual recorded activity (Hazzard & Young, 2004). A model would then be valid if there is a high comparison and then assist in understanding the connection between stress and seismicity.

### ***2.2.12 Past Mining Studies and Assessments***

Iannacchione et al. (2005) has concluded that microseismic monitoring provides the ability to assess the stability of roof rock and that information obtained can identify progressive, episodic, and continuous rock failure processes. Three monitoring sites were examined, each with differing collective seismic characters that were a result of the interaction between mining, geologic, and stress conditions. Progressive rock failures in which quiet periods of activity are interrupted by a progression of events are determined to “signal the beginning of unstable conditions” (Iannacchione et al., 2005). Episodic rock failures, where most activity signifies the development of a stepped failure surface that later leads to roof falls, can be used as a successful warning tool for falls. Finally, continuous activity which corresponds to the front abutment zone in a longwall panel, acts as a base or “normal” condition that can be used to determine any deviations from normal strata response.

### **2.2.12.1 Hard Rock Monitoring**

The Springfield Pike mine, a room-and-pillar limestone mine in Pennsylvania, was monitored for microseismic activity to analyze roof falls (Gale et al., 2001). Faults with several meters of displacement are present, bedding planes extend over large areas, and jointing at the site is generally wide. The main cause of roof falls was said to be the result of high horizontal stresses which contribute to highly stressed areas after mining. Shear failure, created when a stiff, thin bedding in the roof concentrates a critical amount of horizontal compressional stresses, initiates adjacent tensile bedding plane failures (Gale et al., 2001). This creates a weakness in the remaining intact roof beams. When these roof beams fail, stresses migrate to nearby beams where the process begins again. In all, hundreds to thousands of seismic events created from the shear failures can be associated with one roof fall.

In one recorded instance of a roof fall, a low angle shear had generated three months before extensive microseismic activity began (Gale et al., 2001). A mass of 50 events occurred over a two hour period. Gale et al concluded that these events were caused by “thin beds within the immediate roof failing along bedding and through the intact material.” A quiet period of three hours then precluded another set of 50 events within a 20 minute period which is when it was determined the roof fall occurred. Another two hours of quiet then followed. A final period of high activity then lasted an hour. Over the next 16 hours a constant rate of small events were recorded. This period was associated with the edges and top of the roof fall increasing in size (Gale et al., 2001).

### **2.2.12.2 Longwall Coal Mine Monitoring**

Microseismic research completed by Ellenberger et al. (2001) was done at a longwall coal mine in Utah under several sandstone units with a deep cover of 2,500 ft. (762 m.) A three-dimensional microseismic array of geophones were placed both on the surface and underground to monitor the gob formation and stress redistribution of a longwall district. At the end of monitoring, a total of 13,000 microseismic events were recorded, with 5,000 of those events well enough located to perform analysis.

It was found that events occur both above and below the advance of a longwall face in accordance with the forward stress abutment zone (Ellenberger et al., 2001). The study agreed with prior research where seismic activity is known to generally be mostly in front of the face. It has been inferred that this area is well recorded by microseismic system because of the high

energy release and good transmission characteristics. Events from the gob area tend to be lower energy and have trouble transmitting through the broken rockmass. Most of the events line up with the advancing face, but more events occurred further in front of the headgate than the tailgate. This distribution could have been issues with the velocity model or as a result of initial gob formation. Ellenberger et al. also discovered that as the gob became more established, events became more frequent.

Heasley et al. (2001) studied the same data set from Utah as Ellenberger et al. and concluded that there was a positive linear correlation between seismic activity and face advance rate. Most events recorded were a “direct and fairly immediate response” to the mining process and subsequent stress redistribution. Activity occurred both equally above and below the panel and in advance of the longwall face. There was a larger frequency of larger events with a larger density of small events towards the end of the panel, while in the middle there was a higher percentage of medium sized events. In agreement with (Ellenberger et al., 2001), most of the events came from shear failures in the forward abutment zone that is easily recorded as opposed to tensile failure in the gob.

Alber et al. (2009) analyzed seismic events at a German longwall coal mine through numerical modeling and determined that it is unfavorable to orient a longwall panel in the same direction as in-situ stresses. This can lead to high induced stress. It was also concluded that boundary areas around the gob as well as remnant pillars have the tendency to act as stress concentrators. If strong, brittle strata is present, strain energy may suddenly be released.

Swanson et al. (2008) monitored three underground coal mines in Colorado to differentiate between naturally occurring and mining related events. Magnitudes recorded were from 0 to 3.4, with the six largest events recorded having a magnitude of 2.5 to 3.4.

### ***2.2.12.3 Retreat Coal Mine Monitoring***

The only known microseismic study in a room and pillar retreat coal mine was completed by Descour and Miller (1987) at the Olga Portal No. 2 mine in Caretta, WV. The mine was extracting the Pocahontas No. 4 seam with hard, competent sandstone floor and roof and 500 to 1,500 ft. (152 to 457 m.) of cover. All events recorded by geophones at the site were either from a manmade compressive stress source or a natural tensile stress source that occurred from a rock failure. Sources were differentiated by the distribution and dynamics of small signals located in

front of the maximum p-wave signal of an event. The cause was associated with the creation of local instability that resulted in a differing driving force of the source. The first-half cycle of this signal was similar to that of the main signal and occurred as an instantaneous elastic response failure within the stress envelope. Velocities of the P- and S-waves were found to be 16,200 (4,900 m./sec.) and 8,900 ft./sec. (2,700 m./sec.) respectively.

There were two types of microseismic monitoring activity recorded: primary and secondary. Primary events were caused in direct response to mining. These occurred due to the change in stress in close proximity to mined areas during production times. Secondary microseismic events were detected with no direct relation to the retreat mining cycles. This activity was located away from the active section and/or occurred when production was down. It was inferred that these events were caused by stress changes induced in the major stress system due to mining.

It was also observed that initial wave frequency was typically higher for sources that were closer to higher stress zones such as abutment areas and long singular entries. Waveforms for both P- and S-waves of the same source had a similar sequence of elementary particle velocity signals. Events occurring in the middle of the retreat mining area had lower frequency, which is typical of soft support and a variable stress system. In all waveforms though, signal frequencies decreased over the entire waveform. The polarity was positive for tensile events, where the vertical component of the first ground motion was oriented upwards. When manmade events occurred or when events originated outside of the actively monitored section, the polarity of the waveforms were negative.

As coal blocks were excavated during the retreat process, a very direct, local microseismic response developed in small oblong areas with similar dimensions to a single block. The concentration of events were shifted 50 to 100 ft. (15.2 to 30.5 m.) west or east of the block being mined, parallel to the mine's major joint system nearest the area of local stress concentration.

Events tended to concentrate in certain areas labeled as susceptible to instability. Single small events in many cases were also seen to trigger a large event in higher magnitude. When major instability occurred in the rockmass, primarily before a coal bump, individual waveforms from events tended to overlap waveforms from other events. Larger amounts of energy were also released with a decrease in the event rate just before a major failure.

When events were examined on an hourly basis, “saw-toothed” shaped cycles were identified which corresponded with the initial “bumpcut” of an individual coal block. The event rate peaked around one to two hours after the cut was taken, and decreased at a slower rate with a higher average energy per event. These cycles were observed a few times per day, during the morning and consecutive mining shift, but event rates during the night when there was no mining was minimal. Total daily events were concluded to be related to the mining structure’s elements whose integrity to support was compromised from the mining process on the same day. Increases in event occurrence were proportional to the loading on the nearest barrier pillar.

A ringing effect was observed in the floor and roof as a rock layer separated from the remaining part of entry and horizontally compressed causing a long lasting, decaying noise. This effect was interpreted as a result of a large scale stress concentration in the active mining section.

Problems were associated with identifying P-wave arrival times, causing lower reliability for source locations. Due to the small signals arriving in front of and with the first P-wave, precise arrival times were difficult and in some cases impossible. Such was also the case when waveforms with gradually increasing amplitude arrived at sensors, mostly at more remote locations. The beginning of the waveform would be less than or equal to the noise level, causing it to be masked. Problems identifying S-waves were also similar. Even though the S-waves would typically have amplitudes a few times larger, the beginning of the waves would be hidden by the tail of the event’s P-waves. Because of these issues, the particle velocity peak amplitude of the first half-cycle of either the P- or S-wave was a better use than the first arrival time for source location.

# **Chapter 3: Microseismic Monitoring of a Southwest Virginia Room and Pillar Retreat Coal Mine**

## **3.1 Abstract**

Ground control, one of the key elements in mine safety, is an issue that warrants continuous improvement in the underground coal industry. The United States experienced over 3,300 injuries and 42 deaths between 2006 and 2012 from the fall of a roof or rib (MSHA, 2015). Out of the underground coal mining methods, room and pillar retreat mining lacks significant research to adequately understand the rockmass behavior associated with the process. A microseismic monitoring system was installed in a retreat mine in Southwest Virginia to provide more information about the changing stress conditions created by retreating and ultimately reduce risk to miners. Microseismicity has been proven to be an acceptable method of monitoring stress redistribution in underground coal mines and assist in explaining rockmass behavior (Luxbacher, et al, 2007). An array of geophones was placed underground along a single retreat panel to record failures due to stress redistribution throughout one panel of retreat. These microseismic events were located, and their moment magnitudes were found. An analysis was completed to observe the redistribution of stress and related gob formation throughout the panel's retreat. Expectations for the gob formation were consistent with the distribution of microseismic events. Over 13,000 microseismic events were found in 1.5 months of monitoring. Approximately 2,800 of these events were well enough located to provide analysis of the changing underground stress conditions from the retreat process. On average, recorded microseismic events during retreat produced a moment magnitude of -0.9, with no events higher than a magnitude of 2.0.

## **3.2 Introduction**

Ground control is a major issue in underground coal mines. The “soft” nature of the rock, nearby bedding, and seam depth are just a few of the factors that make coal extraction dangerous. In the United States between 2006 and 2012, over 3,300 injuries (fatal, non-fatal days lost, no days lost) were reported as a result of a fall of a roof or rib in the underground coal mine industry. This represents over 16% of all reported underground coal incidents during this period (MSHA, 2015). Forty-two of these injuries resulted in deaths. In comparison during this same

time frame, underground metal mines had 13.5% (240 injuries) and underground nonmetal mines had 6.7% (55 injuries) of all injuries resulting from the fall of a roof or rib. Over the years, the number of injuries have decreased, but as of 2012 there were still 376 yearly injuries in underground coal mines across the United States (Figure 9).

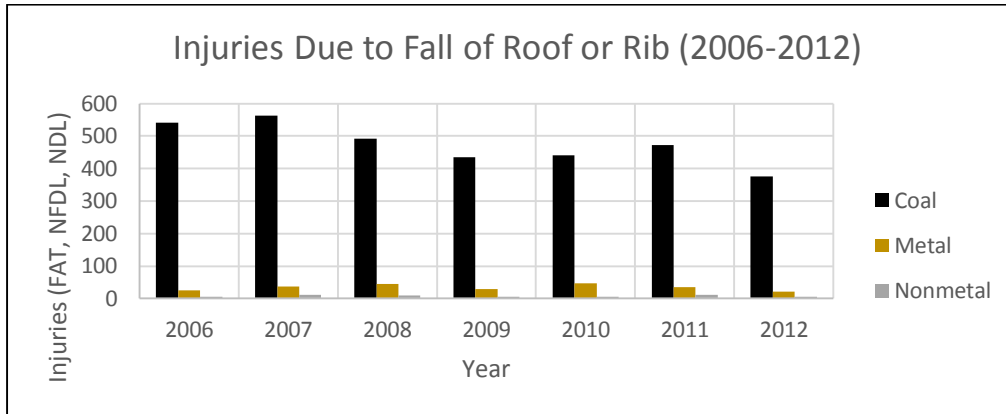


Figure 9: Injuries (FAT, NFDL, NDL) due to the fall of a roof or rib between 2006 and 2012 (MSHA, 2015).

Commonly accepted mining methods, such as longwall and room and pillar retreat, allow overburden to cave. This creates highly variable stress conditions that can be difficult to predict. From both the safety and production point of view, unplanned ground falls resulting from these conditions are unacceptable. Not only can fatalities and injuries occur, but falls can obstruct escape ways, block ventilation, cause stoppage in operations, damage equipment, and cause lost ore reserves. Proper mine design and safe operating procedures are critical to prevent ground control issues from happening.

A common way of determining instability and changing stress conditions in underground mines is to monitor mining-induced microseismic events. A microseismic event occurs when a rock under a critical amount of stress fractures and emits an energy wave of short duration and small amplitude (Obert and Duvall, 1967). Each waveform contains a grouping of elementary wave signals that represent particle velocity initiated by individual pulses of stress wave energy (Descour & Miller, 1987). The energy pulse's shape details the amount of stress released at the source and the effect of non-uniformities in the rockmass along its travel from the source to a microseismic sensor such as a geophone. The polarity of a waveform from both manmade and natural sources can be used to determine whether an event's driving force was shear or compressional (Swanson et al., 2008). Individual waveforms are analyzed to determine the time,

location, and magnitude of a single event. A seismic event with a moment magnitude of typically less than 2.0 is considered “micro” (Spence et al., 1989). Over time, the failure process of a monitored area can be studied from the progression of the located events.

At least three microseismic surveys have been completed and analyzed in longwall coal mines (Luo et al., 1998; Ellenberger et al., 2001; Luxbacher et al., 2007; Swanson et al., 2008; Alber et al., 2009). These studies and analyses verified that microseismic monitoring is a useful tool for understanding stress redistribution in an underground coal mine setting. In contrast, room and pillar retreat mines have had only one published microseismic study. This study, completed in 1987 by Descour and Miller, monitored various parts of a retreat mine section over a 10 month period. The mine layout however was not the same as what is currently found underground. Modern rectangular retreat panels, which incorporate five to seven entries encompassed by barrier pillars on both sides, were not employed. Instead, an entire section of the mine was extracted. Much smaller barrier pillars, approximately the size of 10 production pillars, were placed in vital areas of the section.

This research involves the microseismic monitoring of a room and pillar retreat coal mine panel throughout the retreat process, as well as approximately two months of development for the next panel in the section. The mine site was located within the Jawbone coal seam in southwest Virginia. Retreat data was collected for approximately 1.5 months with the use of eight geophones in the mine roof. Six geophones were located along the first entry of the panel and two were placed in the mains. Events were located and their moment magnitudes were found. The magnitudes and locations of the events were compared to the mine geometry and face location to determine where higher amounts of stress were located.

### ***3.3 Site Description***

#### ***3.3.1 General Description***

The microseismic monitoring site consisted of a room and pillar retreat mine located within the Jawbone coal seam in Southwest Virginia. Monitoring occurred during the retreat of Panel 2D, shown in Figure 10, which is the fourth panel in the south section of the mine. Approximately one-quarter of a subsequent panel’s development, Panel 2E, was monitored as well. Panel 2E is located southeast of Panel 2D and is the fifth panel in the south section of the

mine. The mine works three shifts, 24 hours per day, usually five days per week. First and second shifts are used for production, while the third shift is used for maintenance.

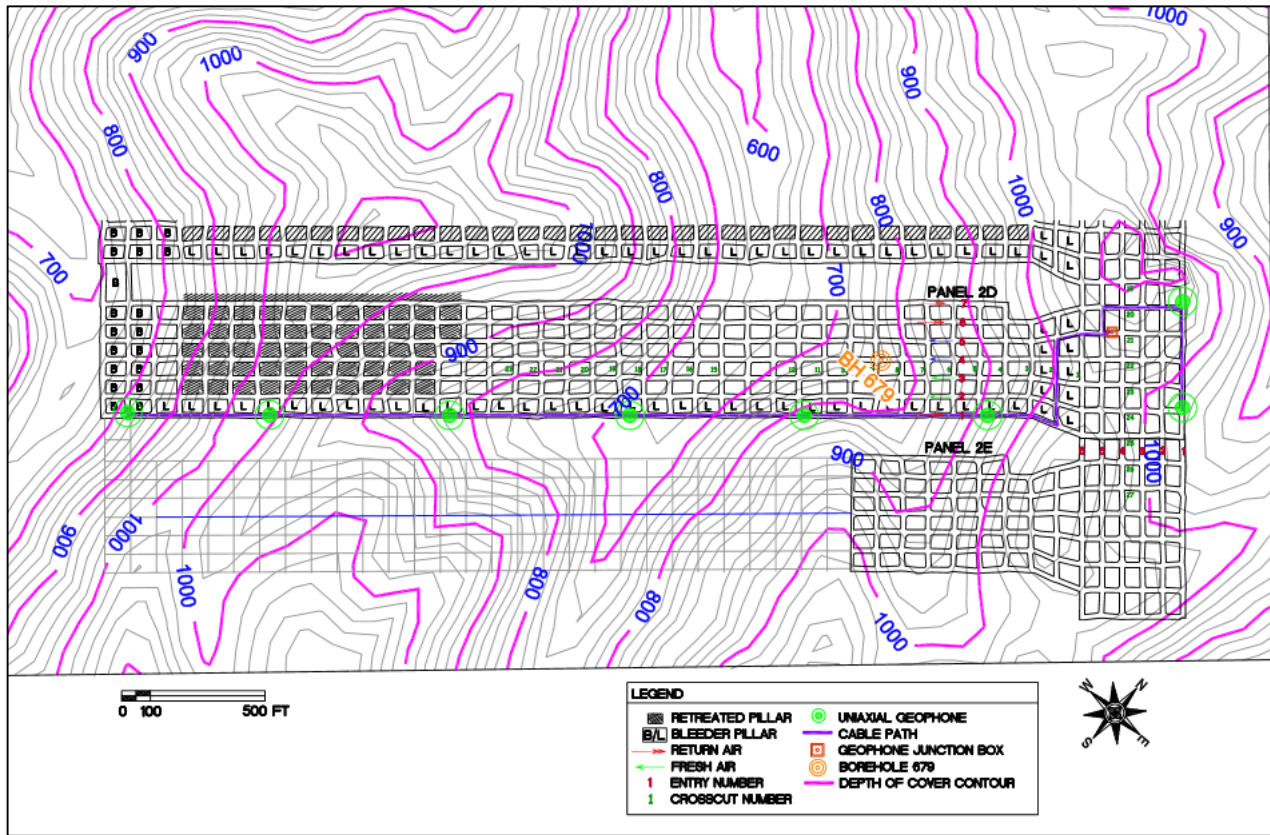


Figure 10: Depth of cover contour of Panels 2D and 2E with partial retreat. Geophone locations, cable paths, and Borehole 679 is marked.

Panel 2D is 3,400 ft. (1040 m.) long by 400 ft. (120 m.) wide. The panel was developed in the direction of S49°W and retreated N49°E. A seven entry design was used, with each entry having a width of 18 ft. (5.5 m.) and a cut height of six to seven feet (1.8 to 2.1 m.). The average coal thickness is about five feet (1.5 m.) with six inches (15 cm.) of parting. The rest of the cut height comes from cutting into the rock overlying the coal. No top rock was removed when extracting the pillars on retreat, so the void between the roof and floor where pillars once stood was approximately 10 in. (25 cm.) lower than the cut height in the entries.

All pillars in the panel were rectangular, measuring 70 by 45 ft. (21 by 14 m.). In total, the panel stretched 38 pillars long by six pillars wide. Center-to-center spacing was 90 by 65 ft. (27 by 210 m.). The line of pillars between the first two entries in the panel (from left looking inby), as well as the last two rows of pillars most inby, were left in place during retreat. A barrier

pillar, measuring 130 ft. (40 m.) wide, stands between the preceding retreat panel to the northwest, Panel 2C, and Panel 2D. Panel 2E has been designed with the same geometry as Panel 2D. A 150 ft. (46 m.) wide barrier pillar has been left between these two panels.

Pillars are extracted during retreat starting from the seventh entry, directly adjacent to the barrier pillar separating Panels 2D and 2C. Mining then subsequently continues southeast towards the first entry, as shown by hatching in Figure 10. The mine employs a “Christmas Tree” cut pattern while extracting pillars, with an outside lift (slab) cut of 32 ft. (9.75 m.) placed into the barrier pillar. This leaves a caving span of approximately 370 ft. (113 m.) wide.

Panel 2D has a high level of topographic relief, with a depth of cover ranging from 600 to 1,000 ft. (180 to 305 m.). A valley with a small stream is located near crosscut 15, while mountain ridges lie at crosscuts 1 and 32. Both of these areas are beneath 1,000 ft. (305 m.) of cover. The monitoring area of the development of Panel 2E ranged from approximately 850 to 1,000 ft. (260 to 305 m.) of cover, with greater depths towards the southeast side and beginning of the panel. There were no structures located above either panel throughout retreat. Contours for the depths of cover for Panels 2D and 2E are displayed in Figure 10.

### **3.3.2 Panel Geology**

The coal from the Jawbone seam at the mine site is approximately five feet thick and of bituminous rank. The seam at the panels has an average dip of 1.7% towards N16°W, with a strike of N74°E. The face cleat is orientated at N68°E, while the butt cleat lies at N15°W. Principal stresses have not been gathered at the site. The coal contains 5.12% ash, has a sulfur content of 0.77%, and is 25.95% volatile matter. Throughout the two panels, the Jawbone seam has been highly fractured. This has attributed to a weakened rib structure that has resulted in rib sloughage of six inches to one foot in most areas where no rib bolting was installed. Rib bolting was completed on four foot centers for approximately one-third of Panel 2D, beginning at crosscut 16 and continuing outby.

A regional thrust fault has created a flat lying detachment fault surface within the coal bed due to lateral movement. As a result of faulting, drag folds, which are slickensided inclined fractures, are present in the seam itself and lay roughly at 45° angles. Figure 11 displays the occasional partings of the Jawbone seam. These fractures tend to intersect at regular intervals.

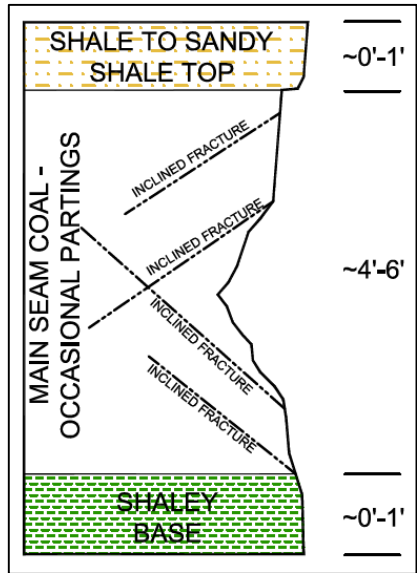


Figure 11: Occasional partings in the Jawbone seam in Panels 2D and 2E.

A corehole was drilled above Panel 2D near the intersection of fourth entry and the ninth crosscut (4-9), which allowed for the determination of overlying strata. Figure 10 on page 35 under General Description displays the location of the hole in relevance to the panel. The hole was drilled approximately one-third of the way between a valley bottom and mountain peak. The corehole intersected the Jawbone seam at a depth of 717 ft. (218 m.) and extended a total of 734 ft. (224 m.). The geology above the panel at the 4-9 location included four main coal seams and alternating layers of shale and sandstone, as shown in Figure 12. Directly overlying the Jawbone coal seam at the corehole was a thin layer of shale, followed by a thicker layer of sandstone.

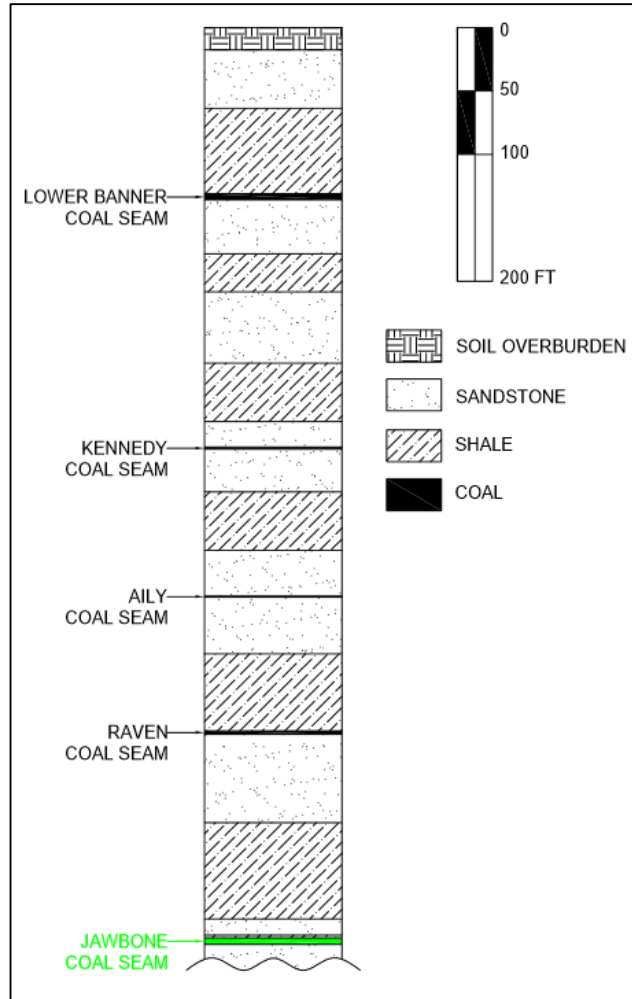


Figure 12: Geologic column of Corehole 679. Total depth: 734 ft. (224 m.).

Figure 13 shows a more detailed view of the strata directly above and below the Jawbone seam. At the corehole location, dark gray, fine-grained shale comprised the first two feet of roof, much of which is removed during mining. A coarse sandstone layer with shale streaks overlies the shale for the next 13 ft. (4 m.) towards the surface. Within the coal, it is observed that there were thin layers of dark gray, fine grained shale. There is also bone coal, which is impure coal with other mineral matter, alternating within the seam. Due to the high degree of in-seam lateral faulting, the presence and thickness of partings within the seam are highly variable and can change from one entry to the next. For the floor rock, dark gray, fined-grained shale extends approximately five feet beneath the bottom depth of the coal. The Jawbone’s leader coal seam, approximately one foot thick, then occurs. This seam is only one foot thick. Another four feet of shale extends below the leader, which is followed by an unknown amount of sandstone.

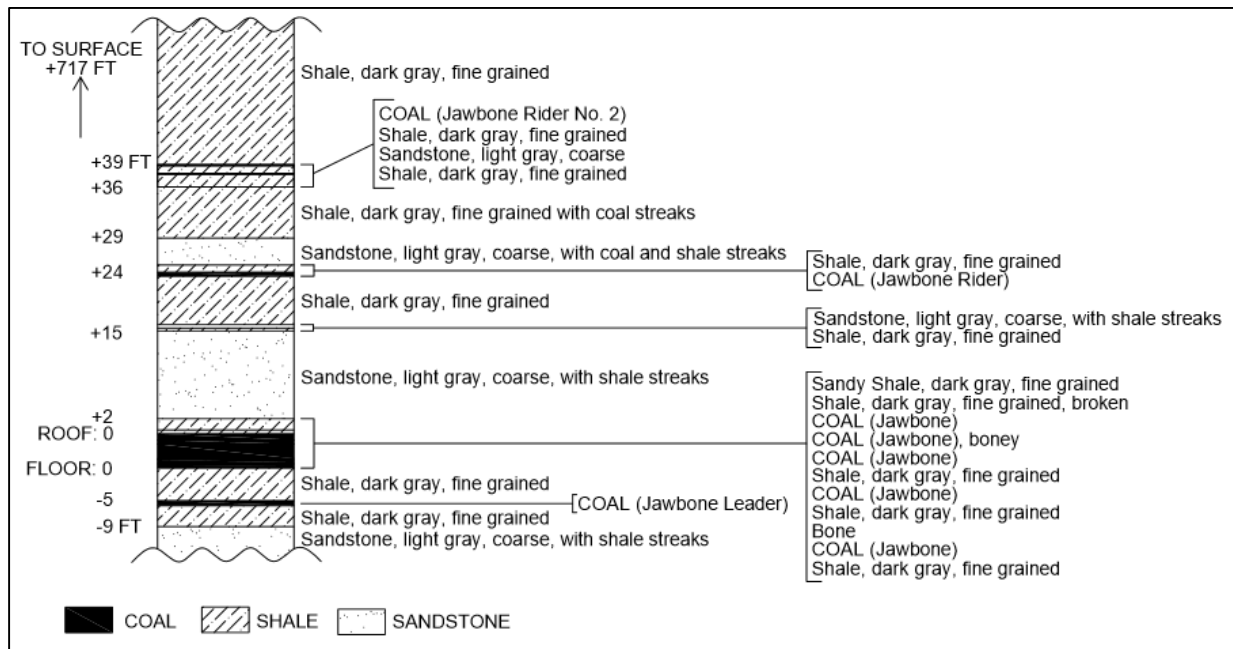


Figure 13: Geologic column of the immediate roof and floor from Corehole 679.

The immediate roof over Panel 2D varied between shale, sandy shale, and sandstone. Over Panel 2D, shale comprised 55% of the roof, while sandy shale accounted for 35%, and sandstone 10%. As shown in Figure 14, the first half of the panel most inby had a shale roof. A sandstone channel then cut across the panel at 40 degrees in a five pillar wide section. The rest of the panel's roof outby was a sandy shale. For the microseismic monitoring period during the development of Panel 2E, most of the roof encountered was from a sandstone channel. Only about two crosscuts had a roof of sandy shale. Visual observations concluded that the roof was generally good, with occasional joints and slickensided roof fractures.

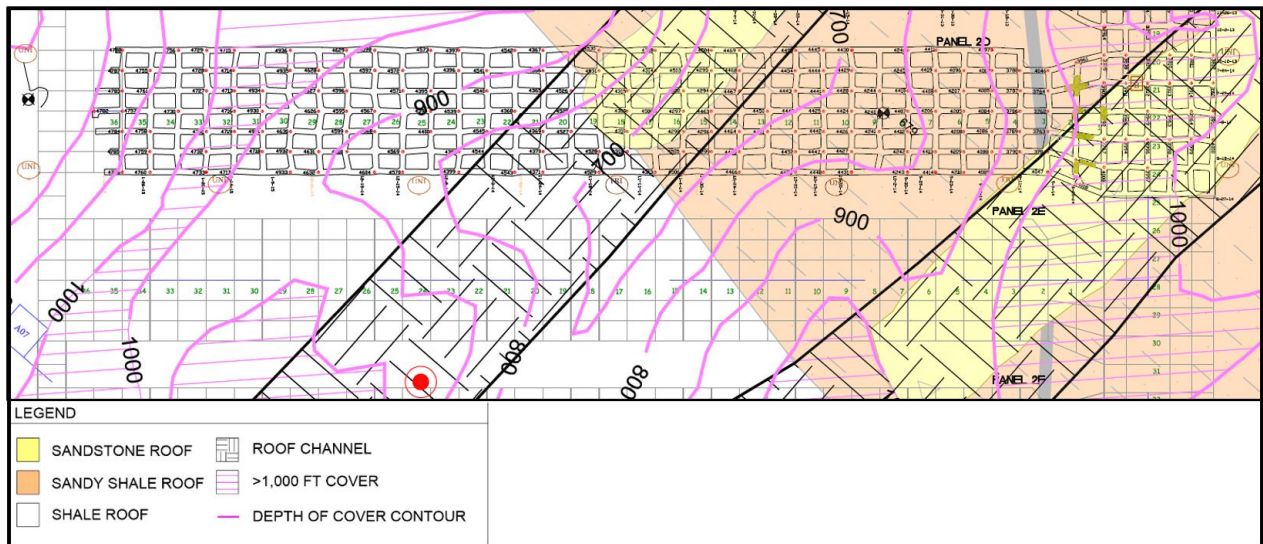


Figure 14: Geologic influence on the retreat panels.

### 3.4 Seismic Monitoring Equipment and Installation

The installed microseismic monitoring system, which was certified as permissible by MSHA, included eight uniaxial geophones that were installed in vertical, 1.5 in. (3.8 cm.) drillholes, 10 ft. (3 m.) above the roof of retreat panel 2D. Geophone locations are shown as green circles in Figure 10 on page 35. Six geophones, approximately 600 ft. (183 m.) (5-6 crosscuts) apart, were placed along entry number one, which was left intact. The other two geophones were placed along the first entry of the mains. The locations of the geophones were selected to provide the best microseismic monitoring coverage of the panel, while not interfering with production. Long-term protection of the geophones for multi-panel monitoring is also possible with these locations since they are installed in a less-traveled entry, away from the caving zone, protected by pillars left between the first two entries.

The uniaxial geophones, with approximately 30 ft. (9 m.) of connected two-pair wire, were installed in the vertical boreholes using a fiberglass installation tool, small paper cups, and roof bolt resin. For each geophone, a small paper cup was cut and lightly taped so that it fit inside of the borehole. The cup was then attached to the top of the geophone with a small bolt and filled with premixed resin. Washers and nuts were used on the bolt to provide an anchor with the resin. The geophone was then connected to the fiberglass installation tool through the use of a modified socket, and then inserted to the top of the drilled borehole. Additional premixed resin

was added below the geophone to ensure proper contact with the surrounding rock by encapsulation. Installation time was approximately five minutes per geophone.

Installed geophones had a frequency response of 15 Hz to 1 kHz to detect signals associated with high frequency microseismic events. Each sensor's total resistance ranged between 1.93 to 2.00 ohms, and had a sensitivity between 40.88 and 44.00 V/m/s.

Separate strands of two-pair, shielded cable ran between each geophone and a junction box located beside of the panel's power center in the fresh air of the mains. Cables connected to geophones in the first entry were bundled together, ran through two stoppings, over a conveyor belt and any existing mine infrastructure, and back to the junction box. The geophones in the mains were bundled, and again ran through two stoppings and a conveyor belt. Careful attention was paid to keep cables away from electrical sources and water pipes in order to reduce interference. Cable paths are shown in purple in Figure 10 on page 35. A maximum cable length of 3,600 ft. (1,100 m.) was used. Cable was hung by zip ties on roof bolts where possible to prevent rib spalling from severing the connection.

The junction box used to house the data recorders, shown as a red square in Figure 10 on page 35 was a NEMA Type 4 enclosure. Inside the box was two 32-bit data recorders, 12 wire terminals with surge protection (six terminals per data recorder), a DIN-Rail Ethernet switch, a 12 VDC power supply, and two fuses. Each data recorder recorded continuously and saved the raw microseismic data to a USB storage device. Timing between the two data recorders was synchronized through the Ethernet switch. The junction box was powered by a 120 VAC connection to the retreat panel's power center, located feet away. A battery backup, lasting approximately 12 hours, was also used to ensure continuous recording, as the mine typically shut down the power center for maintenance during third shift.

### **3.5 Data Collection**

Microseismic data was collected using two 64 gigabyte USB flash drives that were filled approximately every five days. A mine employee would manually remove the flash drive from the data recorder, insert an empty flash drive, and take the full drive to the surface for the collected data to be downloaded to a surface computer. The continuously recorded data was then given in bulk to researchers for processing. If the mine employee was not able to change out the



### **3.6 Data Processing**

Data obtained from the geophones was processed with two seismic event processors. The first processor used the simplex algorithm, which is an iterative location method that uses a geometric pattern to lessen the search volume, to find microseismic events from “triggers”. Triggers occur when software correlates individual sensor waveforms that may have come from one source. If the source is able to be located by P- and S-wave arrival picks, a microseismic “event” is created. Four sub-processors were used in conjunction with the simplex algorithm. The second group processor used source parameters to determine the characteristics of the microseismic sources. Three sub-processors were paired with the standard seismic event processor.

The simplex algorithm began at a sensor array centroid with a starting distance step of 100 ft. (30.5 m.). There was no distance limitation in locating events. Max residuals between the theoretical arrival time pick and actual arrival time pick was set to 0.01 seconds. A least squares estimator was used for misfit calculations. In order for an event to be located, four or more wave picks must have been made. Velocities for the P- and S-waves were respectively set to 10,000 ft./sec. (3,050 m./sec.) and 5,800 ft./sec. (1,770 m./sec.) (Bourbie, 1987). These were estimates from the composition of the surrounding rock mass due to actual wave velocities not being available.

There were four sub-processors that were performed under the simplex algorithm. A baseline processor removed DC offset from the waveform data using a zero level. The zero level was determined by using the first 512 data points of a waveform and subtracting this average from the waveform data. A noise frequency filter also was used to extract the 60 Hz frequency and 9 of its multiples commonly found in power sources. This filter subtracted coherent noise from the waveforms and left the rest of the frequency content intact.

In addition to the baseline and noise frequency sub-processors, a P-wave picker assisted in picking the P-wave arrival times. This sub-processor used a common minimum voltage level for an acceptable P-pick. A 5% minimum voltage peak was selected due to problems receiving the P-wave with the uniaxial geophone system. This places a P-pick on an individual waveform when a data point on a signal trace reaches 5% of the peak voltage. The first pick for a P-wave was selected as opposed to the pick with the highest quality. Noisy data was also rejected to eliminate waveforms with several possible picks. The signal-to-noise ratio was acceptable with

the 5% peak voltage. If seven or more low quality picks were possible in a waveform, then no picks would be made. Picks were also not made if sensors were unsynchronized when recording.

Since problems were encountered determining P-waves within the waveforms, a back polarization sub-processor was used. This processor works best when the largest amplitude signals are the S-wave phase signals. It requires an S-wave arrival pick to determine where a P-wave should be placed. In this monitoring study, strong S-waves were recorded by the geophones. The back polarization method searched the waveform before the apparent S-wave using a function based on polarization and linearity. If no S-wave was present, the maximum energy within the waveform was selected. A signal-to-noise ratio was chosen to be two, where any arrivals with a lower ratio would not be saved.

The second processor used on the raw microseismic data determined the source parameters such as magnitude, energy, and ratio of wave energies based on waveform amplitude, frequency, and duration characteristics. The geometric mean was used in source parameter calculations. A local magnitude estimation was made from the peak particle velocity using the equation:

$$M = 1.515 * \log(d * V) + 1.248$$

where M is the local magnitude, d is the distance to the source, and V is the peak particle velocity. The same average site velocity values as the previous processor were used to determine the source parameters. Data was not corrected for attenuation. Bandwidth and signal-to-noise corrections were performed using corner frequency limits of a minimum multiplier of 0.5 and a maximum multiplier of two. Saturated signals, those that have exceeded the measurement limits of the geophone, were de-weighted. These signals are characterized by DC bias, thus a signal offset ratio of 0.1 was used. If only one P- or S-wave was picked for a waveform, a theoretical pick was added for source parameter calculation.

All geophone data was weighted the same. Low quality geophones were discarded by doing a quality check, which measures the extent of signal decay after its creation. Geophones that exhibit a ringing effect are low quality and experience less signal decay. Geophones with P- and S-wave qualities of less than a value of two were also removed. Those geophones that were more than three standard deviations from the mean of the typical frequency were considered

outliers and removed as well. Geophones that were closer than three wavelengths were considered “near-field” and de-weighted.

Since many source parameter calculations need a value for the integral of the P- and S-wave data, the fraction of P- and S-wave separation was used to find the integral over a window of data immediately following the arrival pick. This window length can be determined by the time separation between the P- and S-wave pick arrival times. The values used for the ratios of the P and S separation were 0.9 and 1.8 respectively. These ratios are in accordance with the high and low frequency limits set in the sensor configuration of the system and reduce the negative effect that integral calculations can have on boosting the low-frequency components of the data. Internal filtering was accomplished by calculating the low frequency limit from the data and using a fraction of peak-amplitude frequency of 0.2. High-frequencies were filtered first. The cutoff value for high frequencies of the geophones was 1,000 Hz.

## ***3.7 Monitoring Results***

### ***3.7.1 Panel 2D Retreat***

Panel 2D yielded 13,183 located microseismic events out of a total of approximately 22,000 triggers throughout the approximately 1.5 month retreat. Events were filtered by having an average error of less than 100 ft. in the x, y, and z directions to determine how many were well-located. The filter also excluded events that had a moment magnitude less than a -3.0, as those events with a magnitude less than this value were incorrectly processed. Out of the total number of triggers, 2,770 events were well-enough located to have an average location error of less than 100 ft. (30.5 m.). Unfiltered event errors averaged 310 ft. (94.5 m.), while filtered errors averaged 56 ft. (17 m.). Figure 17 displays all located events from the top, side, and looking in by the panel that were found when processing, while Figure 18 shows those that had an average error of less than 100 ft.

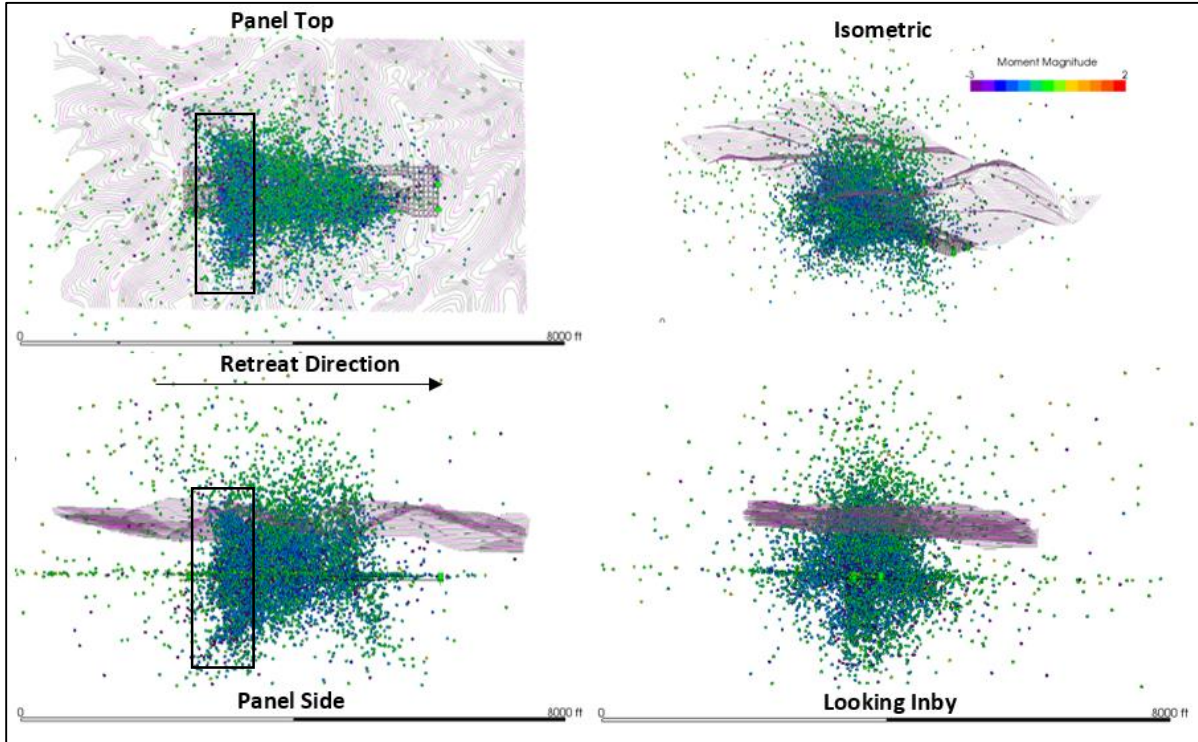


Figure 17: All located microseismic events during Panel 2D retreat. Rectangular outline displays the main cluster of events chosen by hand from the first four days of monitoring.

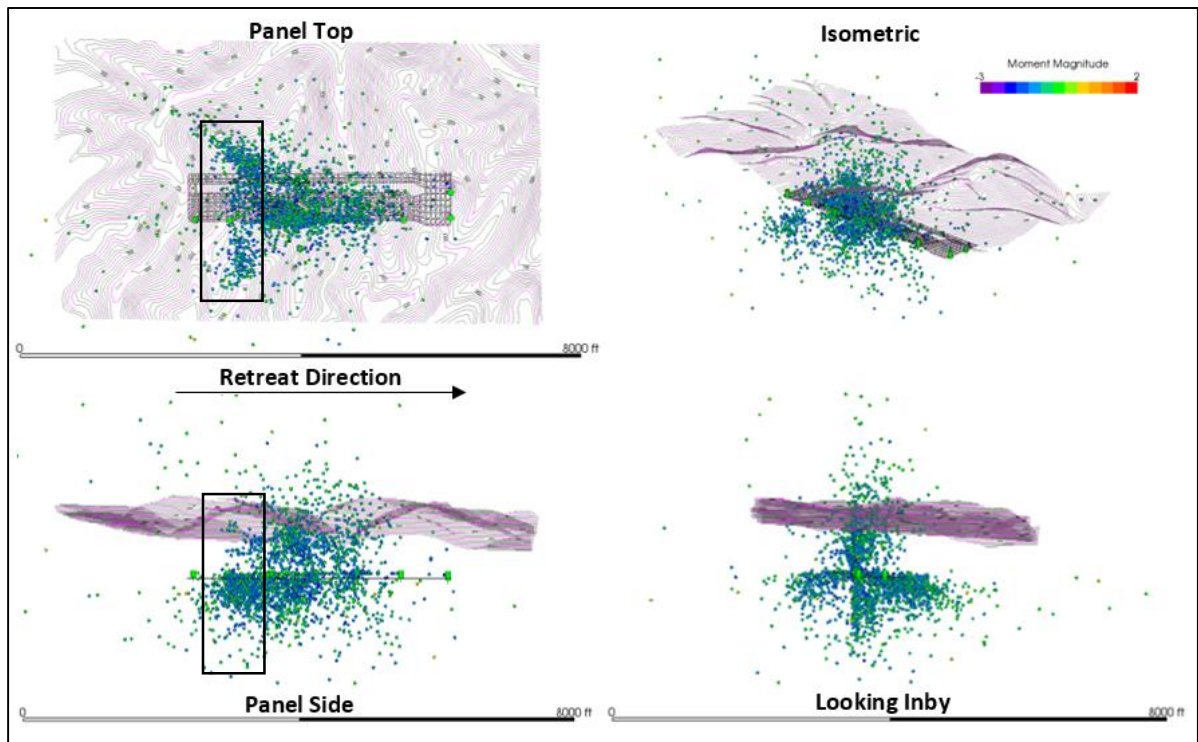


Figure 18: Microseismic events with a location error of less than 100 ft. (30.5 m.) during Panel 2D retreat. Rectangular outline displays the main cluster of events chosen by hand from the first four days of monitoring.

The P- and S-wave arrivals for the collected microseismic data during this monitoring period would have ideally been entirely picked by hand since the software had trouble recognizing the arrival of P-waves. Due to time constraints and the lack of manpower needed to accomplish such a task though, only the waves for the first four days of monitoring were hand-picked. By showing the difference between hand-picking and computational picking, it provides a comparison between more accurate wave picks that were completed by hand, and picks performed by the software with the available equipment during the monitoring period. The hand-picked events appear to be more tightly grouped together in terms of panel length, but more spread in terms of the panel width than the events that were located by computational picking.

The rectangular outlines in Figure 17 and Figure 18 display the main cluster of events that were chosen by hand. It should be stressed that hand-picked events with P- and S-wave arrivals are slightly more precise than those chosen by the computer, but neither are optimal as input wave velocities were constant and roughly estimated. The installed uniaxial sensors were not able to provide a detailed first motion of the P-wave signals which limited results.

When events with an average error of greater than 100 ft. (30.5 m.) are filtered out, many of the events that were picked by hand tend to be located below and beside of the panel, away from pillaring. Although events with low frequencies are expected to occur in the floor and be recorded by the geophones in the roof, the side view in Figure 18 shows hand-picking has a high tendency to place events that were “well-located” below the panel. Figure 18 also shows the tendency of events to be located on the x, y, and z planes of the geophone array when filtering the data. These results are most likely caused by the inaccurate velocity model with constant, estimated P- and S-wave velocities and poor wave arrival picks which did not allow the software to correctly determine the true locations of the events.

Also apparent in Figure 17 and Figure 18 are the number of microseismic events located well above and below the panel. The events located above the surface, known as “air quakes,” are physically impossible, as there is no strata to fracture. Those that occur well below the panel are highly unlikely, as stress redistribution at depths hundreds of feet below the panel is not expected to be at levels that would cause an event. There are also no underlying mine workings at the site to further influence the stress field. Again, the inaccurate velocity model and wave arrival picking contributes to these event locations.

Events picked by hand also tended to have a larger location spread of lower magnitude events than those chosen by the software. Those that had picks chosen by the computer tended to have higher magnitude events further from the panel, with lower magnitudes closer to the retreat. This can best be seen in the top and side views of Figure 17.

To demonstrate the ineffectiveness of picking P-wave arrivals with the large amount of data collected, Figure 19 displays a typical set of waveforms during the monitoring of the retreat of Panel 2D. Each trace indicates the recording of one geophone for 550 milliseconds. The individual traces are from the 266<sup>th</sup> trigger on February 26<sup>th</sup>, 2015. The event was processed the same as all data computationally picked for wave arrivals using the back polarization processing method which estimates the P-wave arrival based on a known S-wave arrival. This method was used because the S-waves were very prominent during the monitoring period and the data contained a lot of low frequencies which makes P-wave phase picking difficult. Trigger 266 contained enough waveforms with a readable seismic signal to be able to calculate a microseismic event. Table 1 displays the event parameters for Trigger 266 that were gathered after processing.

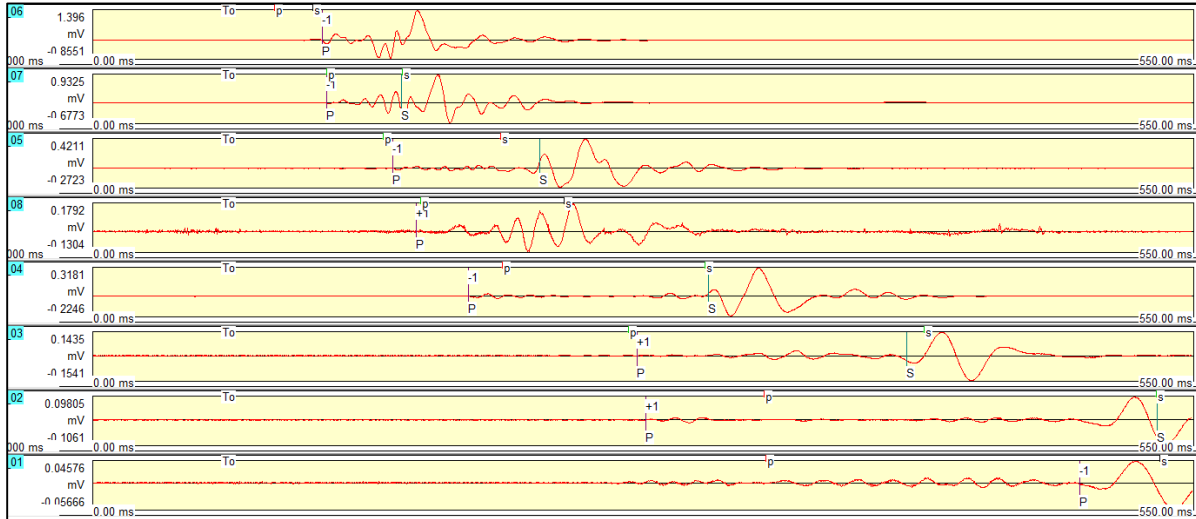


Figure 19: Recorded waveform of Trigger 266 on February, 26th 2015.

Table 1: Event parameters of Trigger 266 on February, 26th 2015

<b>Event Time:</b>	Date	2015-02-26	Time	12:40:51.983
<b>Location:</b>	Northing (ft)*	292323	Elevation (ft)	1336 (Panel+236)
	Easting (ft)*	2149152	Error (ft)	201
<b>Picks:</b>	Sens Used for Loc	6 <i>Uniaxials</i>	P-Picks:	8
		0 <i>Triaxials</i>	S-Picks:	5
<b>Source Parameters:</b>	Moment Magnitude	-0.43	Source Radius (ft)	55.12
	Moment (Mn)	226135376	Static Stress Drop (psi)	3.03
	Energy (J)	23	Apparent Stress (psi)	0.126
	Sens Used for Mag	4 <i>Uniaxials</i>		

\*Company specific coordinates

As shown in Figure 19, the software appears to be able to adequately, in terms of theoretical arrival and visually inspecting the signal trace, pick the P-wave arrival for four out the eight geophones (7, 5, 8, and 3), and sufficiently pick the S-wave arrival for three out of the eight geophones (7 and 4). It is apparent though that all eight geophones were able to capture the event’s waveform and thus an ideal result would be for eight accurate P- wave picks and eight accurate S-wave picks. Table 1 indicates that six geophones were used while processing to determine the event location with a total of eight P-wave picks and five S-wave picks.

There is a fairly large discrepancy between the theoretical arrival time, as indicated with marks above the signal traces, and the actual software picks on most of the individual waveforms. Theoretical arrival times are incorrect because of the inaccuracy of the constant estimated velocity model due to no performed calibration events before or during monitoring. Even though there has been an event calculated, the S-wave picks have forced a solution out of the simplex processor, resulting in a fairly large error. The location of the event is not a complete failure though because sorting individual waveforms with their theoretical arrival corresponds with the geophones visually closest to the source (Figure 20). Also when sorted, the individual waveforms experience a “move-out” of the S-wave phase from the P-wave phase, indicating that they are further away from the microseismic source.

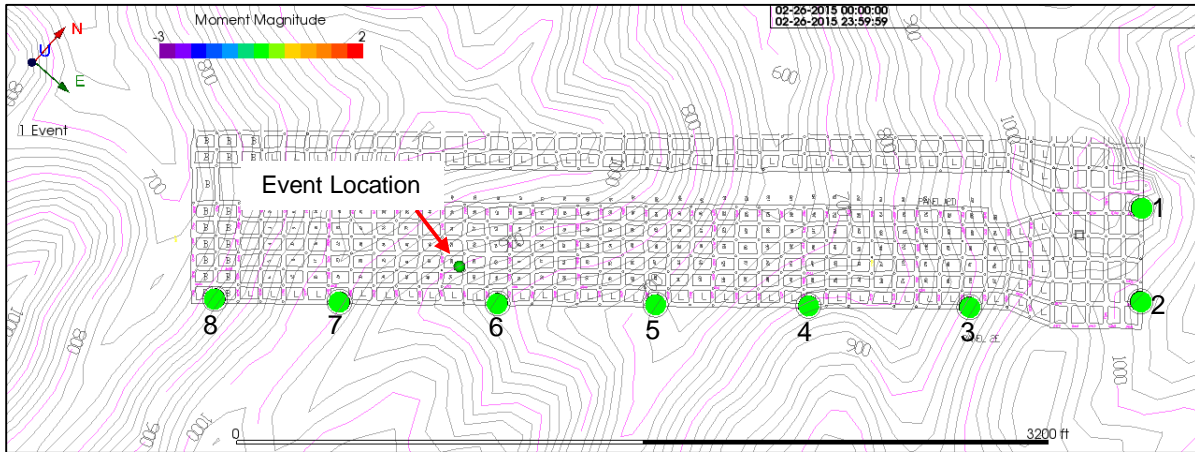


Figure 20: Event location of Trigger 266 on February, 26th 2015.

Another aspect of the P-wave signal is that it is too weak to distinguish its first motion. The initial part of the wave cannot be differentiated from the normal noise of the system. The first motion of the P-wave determines the polarity of the waveform and allows for the failure mechanism that caused the recorded microseismic event to be defined (Swanson et al., 2008).

A plan view of the time progression of events during the approximately 1.5 month long monitoring period of Panel 2D's retreat is shown in Figure 21. All recorded events are displayed on the left, and events with an average location error of less than 100 ft. (30.5 m.) on shown on the right. Each progression groups events from a five to seven day period. Days that are not included contained no data. The difference in event rate is also affected by data collection, as some days were only partially recorded for microseismicity.

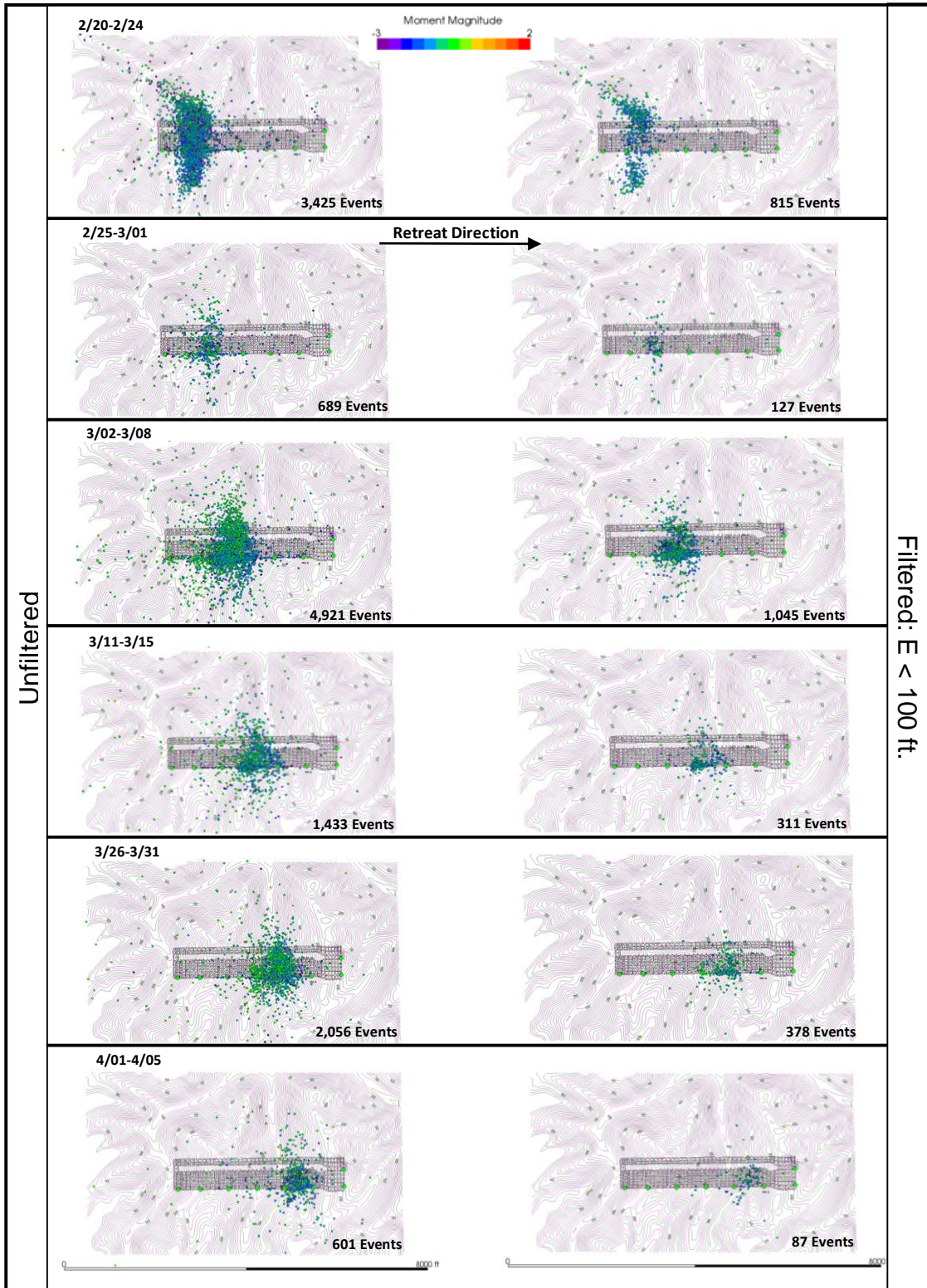


Figure 21: Top view of the time progression of microseismic events during the retreat of Panel 2D. Left progression displays all events, while the right progression displays events with a location error of less than 100 ft. (305 m.).

In general, there is a distinctive cluster line of events progressing in the direction of retreat that is in accordance with the mining rate of approximately two pillar lines every three days. Daily/weekly face locations during the retreat monitoring were not available from the mine site, so exact comparisons cannot be made. It can be assumed by having the cluster of events follow the direction and rate of retreat, the location of events in relation to crosscuts (panel length) can be trusted. Due to the straight line installation of the geophone array, which is able to determine the order of the sensors in terms of distance from the event, this is plausible. The cluster of events are most likely coming from the front abutment loading zone, as this has been confirmed to be the case when monitoring seismicity on longwall panels (Ellenberger et al., 2001; Gale et al., 2001; Heasley et al., 2001; Luxbacher et al., 2007). Seismic signals are easily transferred through this area as it is highly stressed and the strata is not yet loosely broken as in the gob. Any microseismic activity within the side abutment zones could not be confirmed because of the lack of confidence in locations in accordance to panel width. During the period of February 20<sup>th</sup> to February 24<sup>th</sup> though, the hand-picked, filtered data showed a higher concentration of events originating from the “tailgate” side of the panel, which has known higher stresses due to the previously retreated panel (ARMPS, 2013).

The first line of the event cluster appears four crosscuts outby the first pillars retreated. Since data collection did not begin until approximately a week after pillaring began, monitoring more than likely missed the initial caving event. There is a higher percentage of triggers that produced events in the first progression (February 20<sup>th</sup> to February 24<sup>th</sup>) because these triggers were hand-picked, allowing for more P- and S-wave arrival picks to assist the simplex processor in determining a location. Again, it is apparent that hand-picking waveforms also yielded a higher percentage of lower magnitude events than when they were computationally chosen. When filtering according to an average location error of less than 100 ft. (30.5 m.), 20% of computationally picked events remained, as compared with 24% of those hand-picked.

### **3.7.2 Panel 2E Development Results**

The monitoring period during the development of Panel 2E, lasting approximately two months, yielded 515 total events. All waveforms were computationally picked for arrival times. While event rates are expected to be less during development than in retreat, the development monitoring was more intermittent with 40% of the days not resulting in any data. Figure 22

shows the time progression of events for both the top and side views of the Panels 2D and 2E during development. The face locations, which the mine site was able to provide during development, are shown by the red lines. Filtered events due to average location errors are not shown, as there were too few events (61) to provide any visual details.

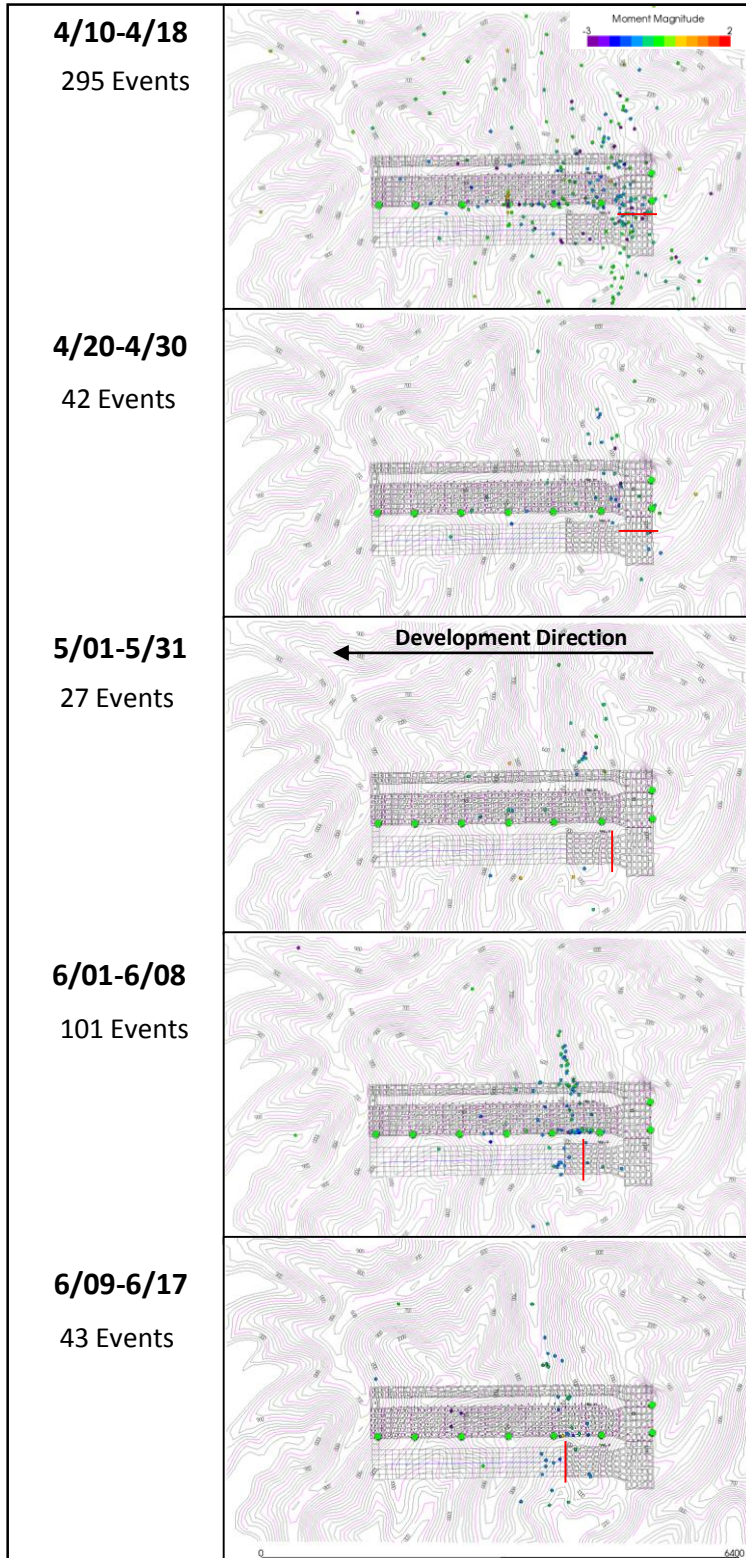


Figure 22: Top and side views of the time progression of microseismic events during the monitoring of Panel 2E's development.

As with monitoring the retreat process, development monitoring also allowed the face to be tracked over time by identifying which crosscut events were originating from. The mine site was able to provide a more detailed schedule to assist in viewing results, breaking down advances in periods of two to six days. Development of the mains began on April 11<sup>th</sup> and continued until May 15<sup>th</sup>. Panel 2E began development on May 16<sup>th</sup> and monitoring ceased on June 17<sup>th</sup>.

There is a clear progression of events moving in the direction of development that coincide with known face locations while mining Panel 2E. The clearest representation of an event cluster is the period of June 1<sup>st</sup> through 8<sup>th</sup>, where a cluster is just in front of the face. Events were not able to be located well-enough in reference to elevation to determine if they originated from the cutter head on the continuous miner, or if they were induced by the rock mass. Most events during all time periods were placed by the software within the area of Panel 2D, where the geophone array was located. Again, there is evidence in Figure 22 that shows events tended to be placed by the software in a straight line along the array of geophones. This can largely be seen in the last two time progressions.

It is also noticeable in Figure 22 that during the first time progression of development monitoring between April 10<sup>th</sup> and April 18<sup>th</sup>, a significantly greater amount of events occurred during a nine day period than subsequent periods of an equal to or longer lengths. This can possibly be attributed to the final stress redistribution of Panel 2D once retreat was complete.

## ***3.8 Monitoring Analysis***

### ***3.8.1 Panel 2D Retreat Analysis***

To analyze the microseismic data gathered during the retreat of Panel 2D, event rates per hour (Figure 23) and moment magnitude (Figure 24) were plotted against time. Each plot uses Greenwich Mean Time (GMT), which is five hours faster than Eastern Standard Time (EST) where this data was recorded. The panel was paused during retreat from March 16<sup>th</sup> until March 20<sup>th</sup>. This period is shown as a black outline in both figures. While noticeable gaps appear in the data collection, several observations can be made concerning the progression of event rates and resulting magnitudes.

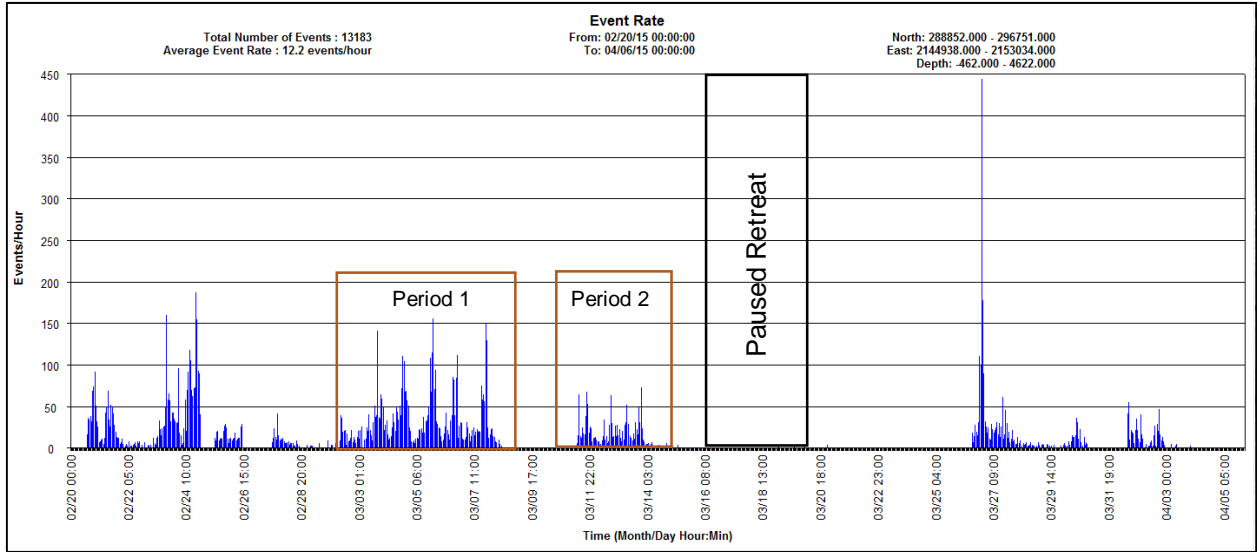


Figure 23: Event rate (per hour, GMT) for all located events during Panel 2D retreat.

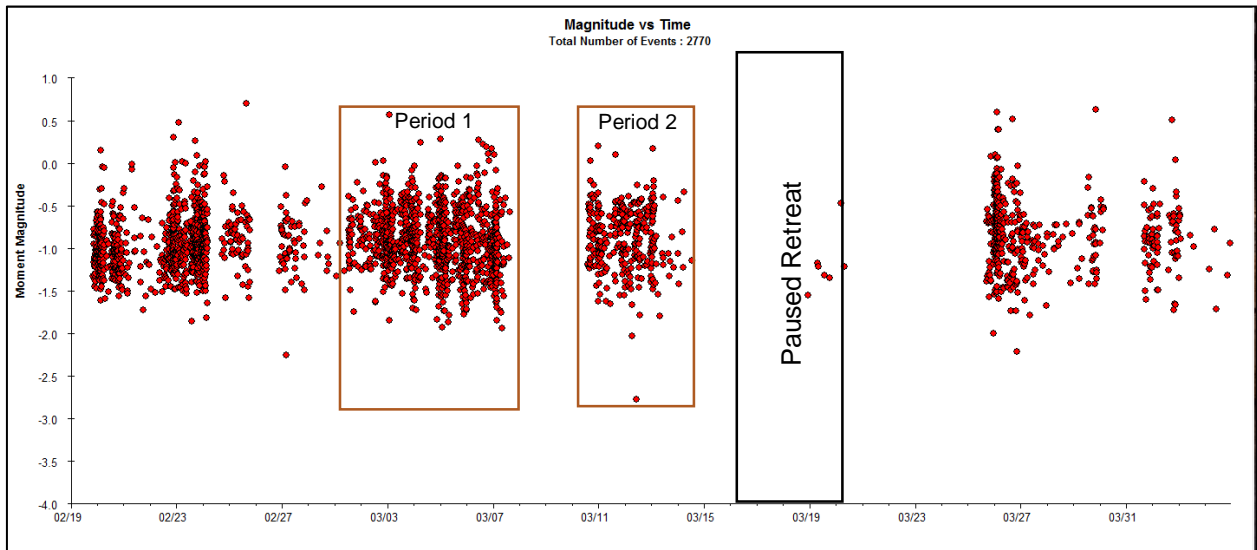


Figure 24: Magnitude verse time (GMT) chart for all located events during Panel 2D retreat.

Two event per hour peaks occur on fully monitored days. One hourly event rate peak occurs during the early morning hours of third shift, typically between 3:00 am and 7:00 am EST. The second daily peak occurs in the afternoon, between 12:00 pm and 4:00 pm EST, and is larger than the previous. At the mine site, third shift is set aside for maintenance while first and second shifts are used for production. First shift begins physically mining at approximately 7:00 am and continues until 2:00 pm EST. Second shift begins mining at 3:15 pm and continues until

around 11:20 pm EST. One full pillar line is typically mined every day. The shifts typically switch halfway across the face in entry five as mining progresses from entry seven to entry two.

Before the larger peak in event rates, events per hour tend to exponentially rise daily until a maximum is reached, then sharply fall, resulting in a cycle that exhibits a skewed left appearance. Peaks during the afternoon hours are possibly attributed to a buildup of stress as mining progresses halfway across the face, the pause for shift change, and the continual mining across the face towards entry two, resulting in a critical failure point in the roof that releases the stress accumulation. Exact face locations and better wave arrival picks are needed though for indisputable conclusions. Figure 25 (period 1) and Figure 26 (period 2) show closer views of the peak cycles with their respective peaks identified by time. When viewing the magnitude verse time plot in Figure 24, the larger afternoon peaks tend to have more spread in magnitude than the peaks that occur during the morning hours and other monitoring.

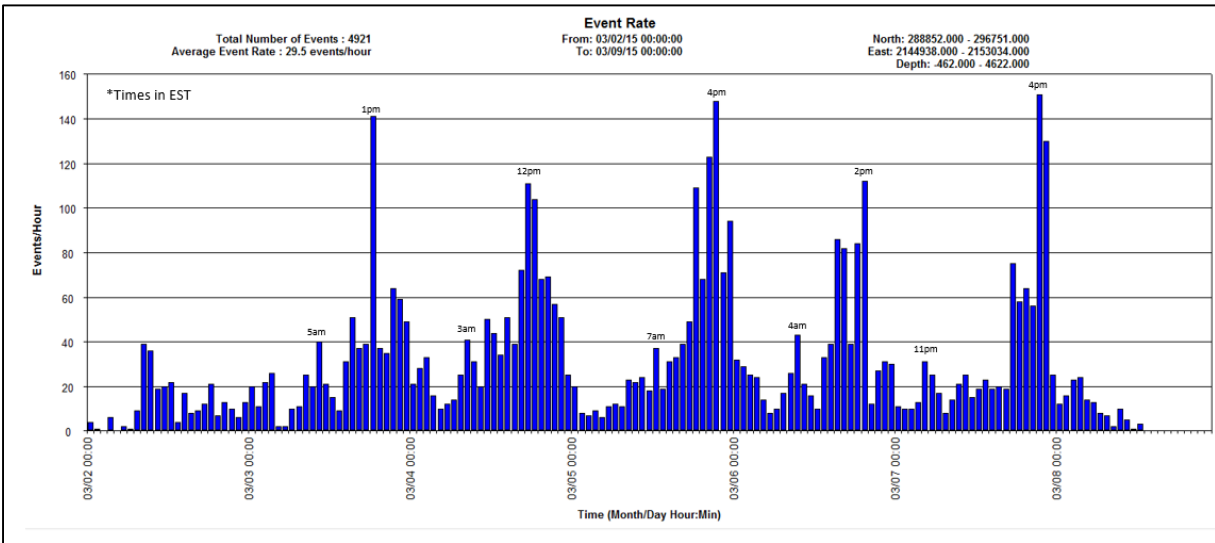


Figure 25: Event rate peaks (period 1) with noted times in EST.

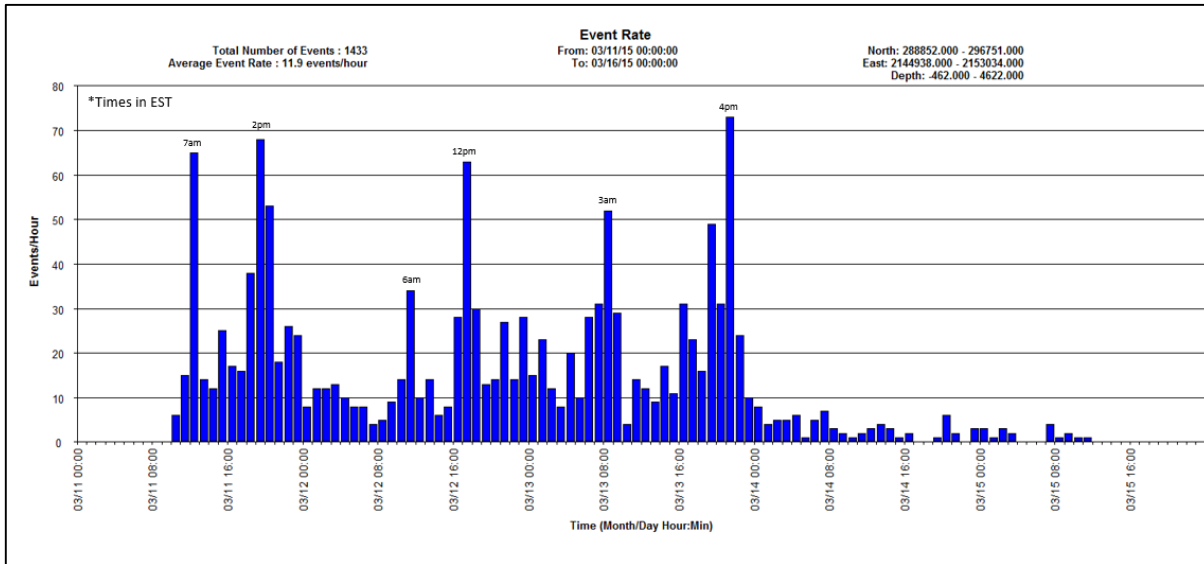


Figure 26: Event rate peaks (period 2) with times in EST.

Figure 23 also displays a noticeable change in event rates per hour between the continuous monitoring periods of March 2<sup>nd</sup> to 8<sup>th</sup> and March 11<sup>th</sup> to 15<sup>th</sup>. At an overall mining rate of approximately two pillar lines every three days, retreat would have changed from under a more brittle shale roof, to a mixture of sandstone and sandy shale on or around March 10<sup>th</sup>. A map detailing estimated face locations for the two periods with relation to roof geology is found in Figure A-1 of the Appendix. The event rates per hour between March 2<sup>nd</sup> and 8<sup>th</sup> were much higher than those experienced between March 11<sup>th</sup> and 15<sup>th</sup>. Although not accurate because of P-wave identity issues, event magnitudes shown in Figure 24 are not comparably different for the two periods of differing geology. A statistical analysis determining if the moment magnitudes between each monitoring period is different is shown in Appendix C.

The depth of cover between the two periods examined are slightly different, but may have still influenced results. Between March 2<sup>nd</sup> and 15<sup>th</sup>, the depth of cover ranged from 750 ft. to 950 ft. (230 m. to 290 m.), compared to a range of 700 ft. to 800 ft. (213 m. to 244 m.) between March 11<sup>th</sup> and 15<sup>th</sup>. Furthermore, no conclusions could be made when retreating under 1,000 ft. (305 m.) of cover in crosscuts 31 to 33 because of inconsistent data collection and unknown exact face locations.

Another element of Figure 23 is that it displays one hour of an extremely high rate of events on March 26<sup>th</sup>. There were 444 events that occurred between 5:00 pm and 6:00 pm. It should be noted that Figure 24 displays that the magnitudes of these events were roughly similar

to those experienced during other periods of retreat. When an estimation of the face location (crosscut 12) on this day is overlain on the roof geology and depth of cover, no abnormal observations can be made (Appendix B). Pillaring was taking place under a sandy shale roof at 700 ft. to 800 ft. (213 m. to 244 m.) of cover. Retreat would have been outby the sandstone roof channel by two to three crosscuts. A large section of hanging roof could have failed, possibly causing the large peak in events per hour, but documentation of individual caving events was not available from the mine site. The five day pause in retreat would not be expected to influence this high event rate, as pillaring began again on March 20<sup>th</sup>, six days before the high event rate was encountered.

The magnitude distribution chart showing the retreat events that were located with an average error of less than 100 ft. (30.5 m.) is displayed in Figure 27. These 2,770 events ranged from a moment magnitude of -2.8 to 0.7. The events are approximately normally distributed, with a mean of -0.91 and a median of -0.90. The standard deviation of the moment magnitude of the events is 0.36. Descriptive statistics for the filtered and unfiltered data are found in Appendix D.

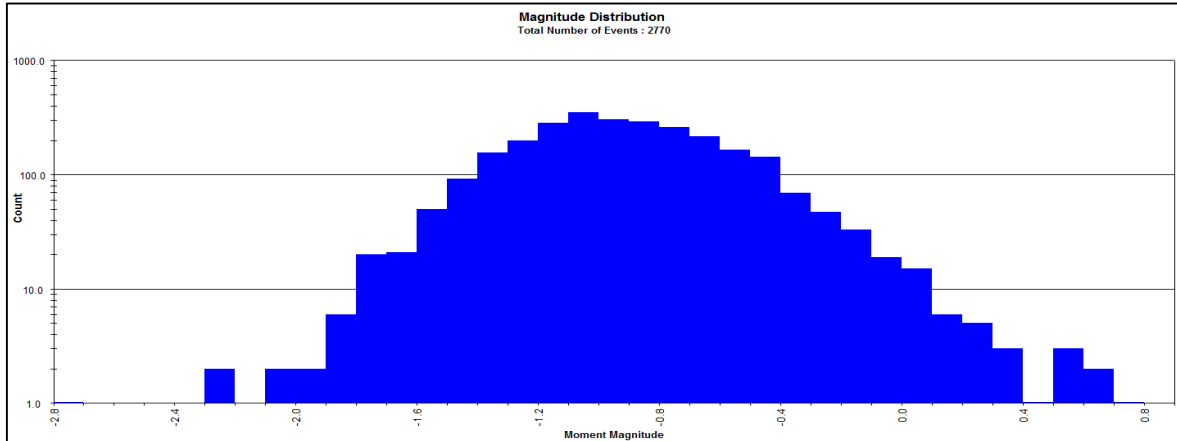


Figure 27: Magnitude distribution chart for events with an average location error of less than 100 ft. during Panel 2D retreat.

Figure 28 displays the inter-event distances for events with a location error of less than 100 ft. (30.5 m). An inter-event distance is the point-to-point distance between two consecutive events. The black line on the figure shows the panel width of 400 ft. (122 m.). It can be inferred that even though the chart is skewed to the right, indicating that shorter distances are more prevalent, a much higher percent of the distances are longer than the panel is wide. This shows

that most microseismic events occurring during the retreat of Panel 2D are independent events not directly caused by previous activity. Due to the uncertainty of processing the data as a result of poor P-wave arrival identification, this representation of the data may not be correct. Rebound effects, where roof falls create a microseismic signal when contacting the floor, could be recorded by the microseismic system and influence Figure 28, but events are not well-enough located for analysis.

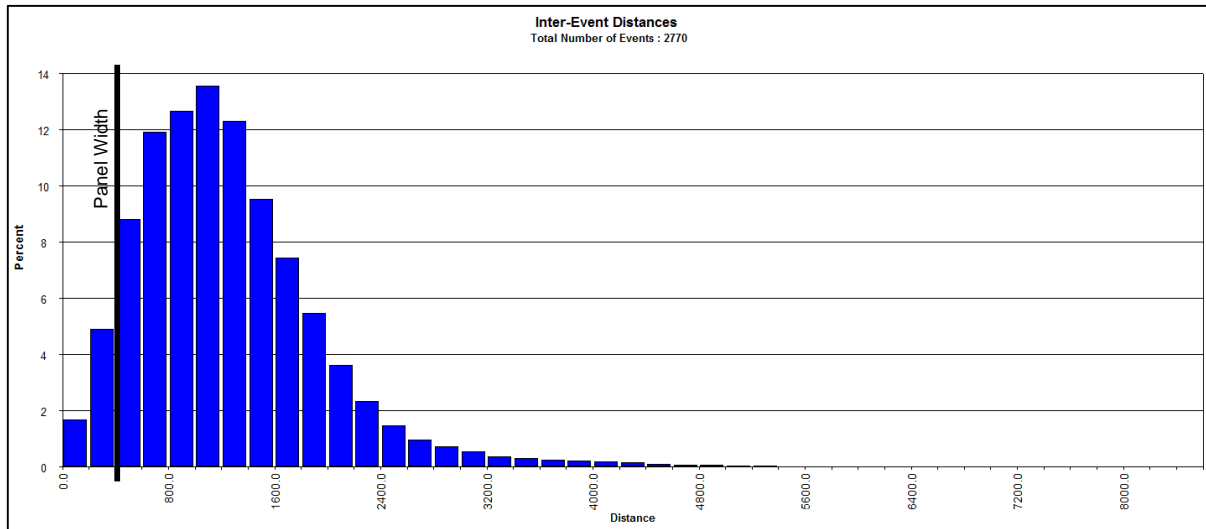


Figure 28: Inter-event distances for events with a location error of less than 100 ft. (30.5 m.) during Panel 2D retreat.

Most microseismic events during retreat typically took place between the hours of 7:00 am and 6:00 pm EST, as shown in Figure 29. This time period coincides with the shift schedule at the mine, where first and second shifts are used for production, and third shift is used for maintenance. At 7:00 am, the total number of events increased at a faster rate than they decrease after 6:00 pm. No apparent change occurred between the first and second shift change. The time of day plot shows expected results. In the morning, any built up stress from the break in mining the night before would be released quickly as production began, causing a higher total number of events. The decrease in the total events after 6:00 pm correlates with the daily event rate peaks shown earlier in Figure 23. Panel stresses during this period would lessen as the major caving events for the active pillar line would theoretically have already occurred. Figure 29 also displays slight increases in microseismic activity between the hours of 10:20 pm and 12:40 am EST. This could possibly be from a final caving event as a pillar line is fully extracted. Another increase in total events occurred between 3:00 am and 5:40 am EST during third shift when there

is no production. Increases could be due to a correlation with typical times of belt moves and other maintenance activities. Due to unavailable records, the causes of both increases in activity cannot be confirmed.

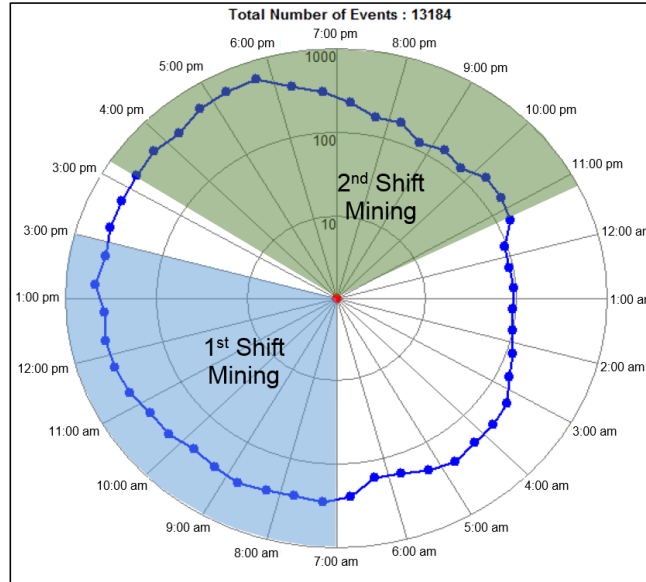


Figure 29: Time of day plot for all located events during Panel 2D retreat (times in GMT).

### 3.8.2 Panel 2E Development Analysis

When examining hourly event rates during the monitoring of the development of Panel 2E (Figure 30), it was found that the first few days after pillaring ceased event rates were similar to those observed while retreating. Data was unavailable between April 5<sup>th</sup> and 10<sup>th</sup> though to make a full conclusion of the event rate trend after the retreat was completed. Throughout the development monitoring period, data collection was also too inconsistent to provide any major details. Event rates though were found to rarely surpass 10 events per hour, with most hours having a single digit rate of events. Peaks were observed normally on first shift, during the late morning hours, just before noon. A small spike of events was also observed between June 1<sup>st</sup> and 8<sup>th</sup>. From this monitoring period on, event rates per hour appear to be higher than the previously collected data which could be attributed to a change in immediate roof composition from sandstone to a sandy shale.

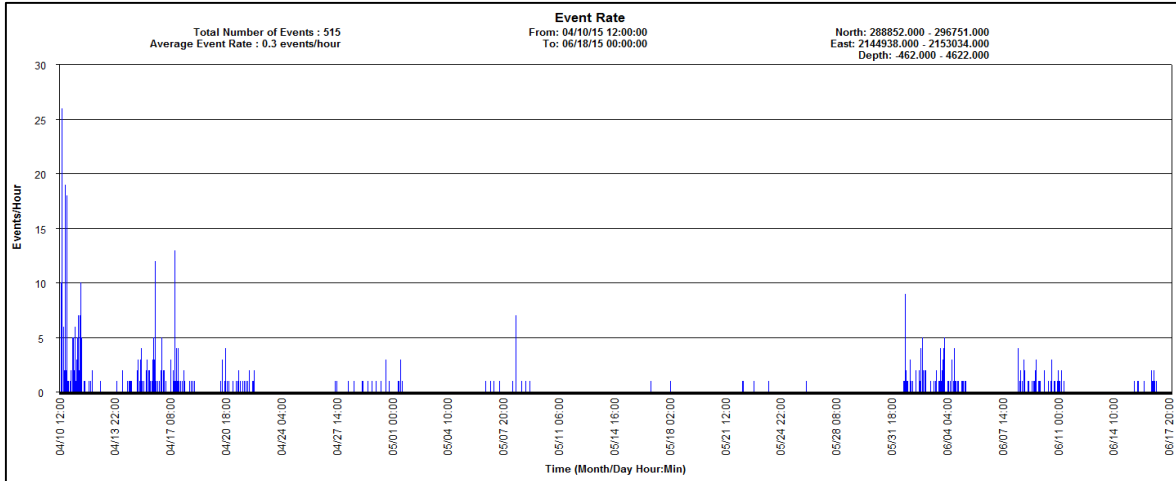


Figure 30: Event rate (per hour) for all located events during Panel 2E development.

While not as defined as the retreat time of day plot, the event time plot of the development monitoring, located in Figure 31, again displays that more events were recorded during production on the first and second shifts at the mine. The time period between 9:40 am and 4:20 pm EST saw the highest number of events.

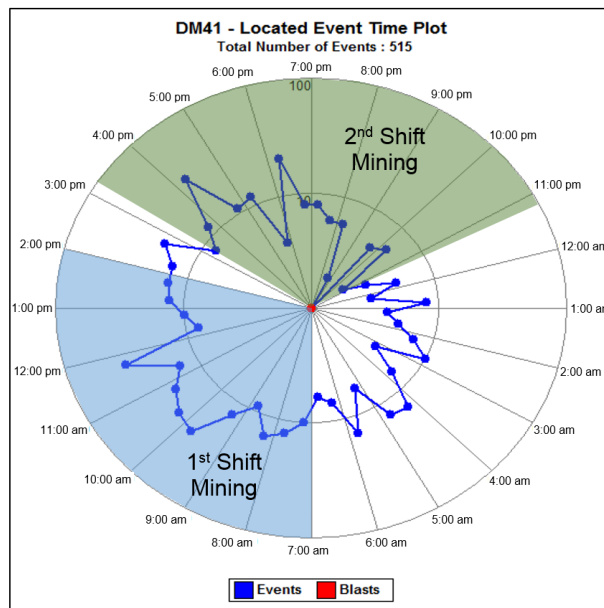


Figure 31: Time of day plot for all located events during Panel 2E development (times in GMT).

Figure 32 displays the inter-event distances found from the events that had an average location error of less than 100 ft. (30.5 m.). While only 61 events fit this criteria, most subsequent events were at a greater distance away than the width of the panel, again inferring

that events did not directly cause other events to occur. Also, some events may still be occurring from the redistribution of stress in Panel 2D, in addition to those being caused by development. The inter-event distance plot may be more skewed to the right by having these two microseismic source areas.

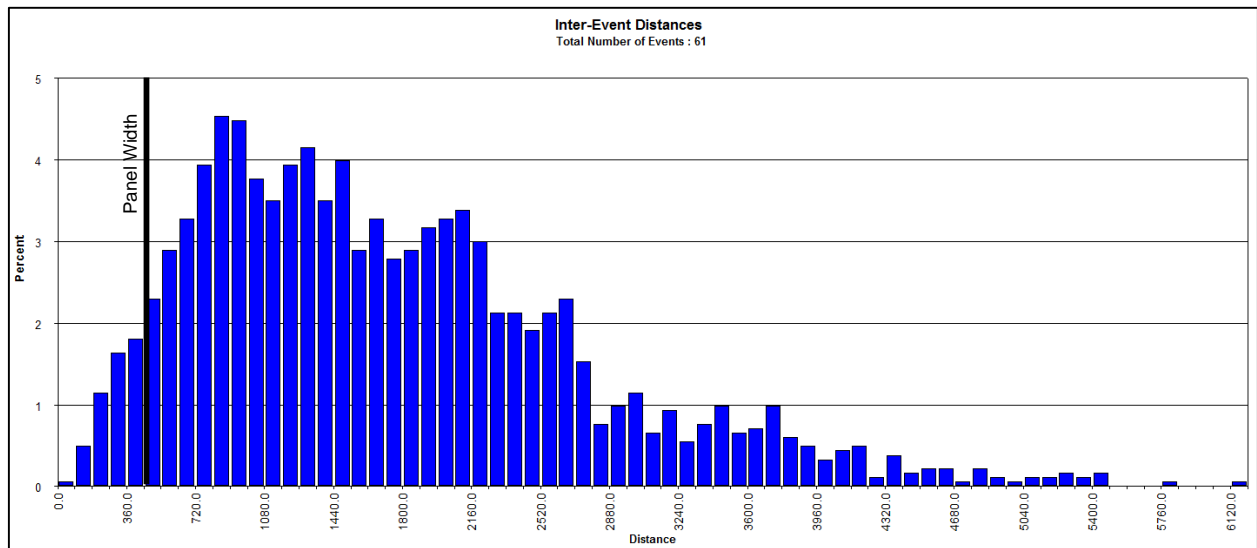


Figure 32: Inter-event distances for events with an average error of less than 100 ft. during Panel 2E development.

Event location errors averaged 488 ft. (149 m.) for unfiltered data during Panel 2E’s development. Higher errors were expected due to the location of the geophone array in relation to the developing panel. An average of 3.70 geophones were able to be used for processing for the development of Panel 2E, compared to an average 4.25 geophones able to be used during Panel 2D’s retreat. Descriptive statistics for both the number of geophones used and errors is found in Table A-1 of the Appendix.

The average moment magnitude calculated for an event with an average location error of less than 100 ft. (30.5 m.) during the monitoring of the development of Panel 2E was -0.62, higher than the -0.91 average observed during retreat. Descriptive statistics for event magnitudes are found in Table A-1 of the Appendix. These results are unexpected, as retreat is typically viewed as producing larger events due to major stress redistribution and caving. The minimum and maximum magnitudes calculated however, were roughly the same between retreat and development. A possible explanation for the difference in processed magnitudes would be that during development, microseismic waves would be well-coupled with solid rock and do not have

to travel through a gob area that would weaken signals. Figure 33 shows that the magnitudes are not normally distributed for the small amount of data collected. Additional monitoring with an improved geophone array is needed to base further conclusions on the moment magnitudes during panel development.

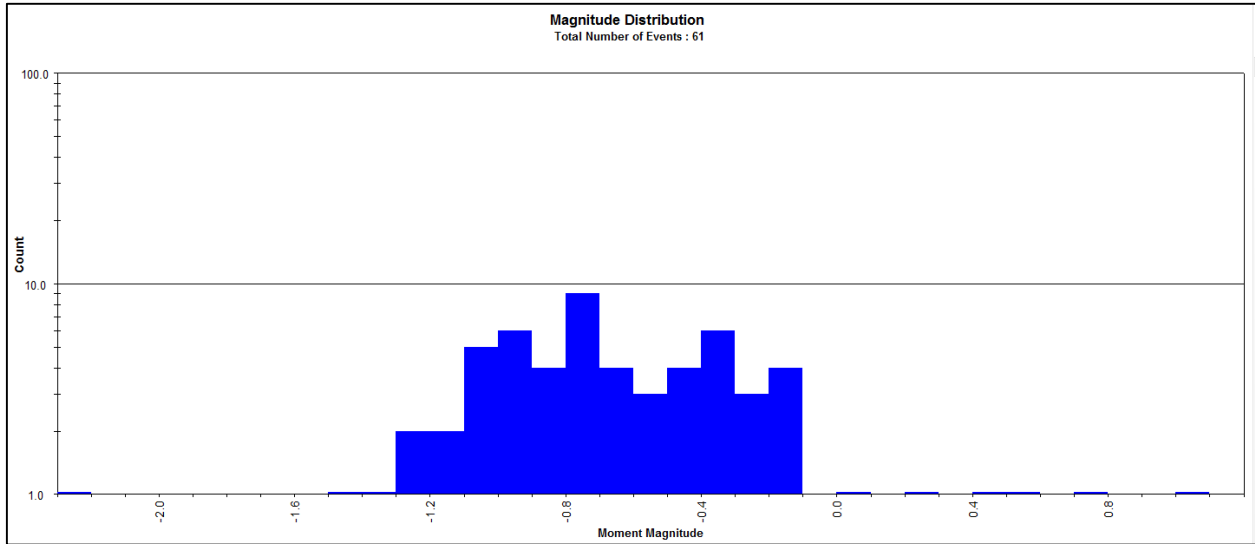


Figure 33: Magnitude distribution chart for all located events during Panel 2E development.

### 3.9 Obstacles

Several obstacles were encountered while installing equipment and processing the data for Panel 2D's retreat. Two triaxial geophones were initially planned to be installed along with the uniaxial sensors in Panel 2D in order to better locate seismic sources due to their three-directional sensing capabilities. A large enough roof bolter drill bit to bore the 2.5 in. (6.4 cm.) diameter holes needed for the triaxial geophones could not be located before retreat began. As a result, the two planned triaxial locations in Panel 2D were exchanged for uniaxial sensors and microseismic signal measurement was limited to the vertical orientation.

This issue further caused problems processing the recorded seismic waveforms. Typically, the primary wave is used to determine the location of the source. Since these waves are compressional, they encountered the vertically oriented uniaxial sensor in the horizontal direction and thus were difficult to identify both visually and computationally. S-waves however were easily recognized. Due to the software not being able to identify the P-waves, the P- and S-waves for the first four days of monitoring were picked by hand. The back polarization sub-

processor previously discussed under Data Processing, which estimated the P-wave arrival time based on the S-wave, was used for processing the rest of the monitoring period.

The geophone array installed above Panel 2D was also not optimal. An ideal array, which typically are installed in hard rock mines, would be three dimensional with geophones located both below ground on different levels and on the surface. In this study's case, geophones were generally installed in a horizontal plane, as there was only one level underground. The mine site was not capable of transferring the gathered seismic data to the surface, so no geophones were installed above ground. The two groups of geophones would have had to be synchronized to ultimately find the magnitudes and locations of events.

P- and S-wave velocities were set at 10,000 ft./sec. (3,050 m./sec.) and 5,800 ft./sec. (1,770 m./sec.) for the entire monitoring period, which is unrealistic. These values were estimates due to not having the ability to perform a system calibration with an event with a known time, magnitude and location. A system calibration would have allowed for better starting estimates for the wave velocities to be more accurate and precise when determining a mining induced source's magnitude and location. Ideally, system calibrations should be performed as often as possible both before and throughout a panel's retreat since stress zones, and thus wave velocities, are constantly changing due to the creation of gob during retreat mining.

High electrical activity was observed in the waveforms during some periods of monitoring. There was no correlation between the time or date of these periods, but most occurred during the development of Panel 2E. The seismic equipment manufacturer recommended keeping cables away from electrical sources, and if possible, cross wiring at 90 degree angles. Both of these installation techniques were possible near the geophones, as they were all located in the panel's returns. However, as the cables progressed towards the junction box, which was beside the power center, the recommendations were not able to be strictly followed. This could have been a possible cause of voltage spikes received in the affected waveforms.

A large problem experienced during the monitoring period was the collection of data. Since microseismic data was being continuously recorded, mine employees had to consistently remove and replace flash drives connected to the data recorders before the drives began overwriting themselves. If a designated employee had time off or was busy, the data could easily be overwritten a few days. Data collection options for the site were limited. Other options such

as connecting a laptop to the data recorders could have lost more data, even with a battery backup. If power had been completely lost to laptops for any amount of time, they would not automatically power back up and start recording. Large external hard drives were tried with the system but would not allow recording. As discussed, sending the data to the surface via a hard line was not possible due to the mine's infrastructure.

### **3.10 Conclusions**

A room and pillar mine panel in the Jawbone coal seam in Southwest Virginia was monitored for microseismicity during retreat. Roughly one-third of the development of the mine section's subsequent panel was monitored as well. Eight uniaxial geophones were used to record events. Two were placed 10 ft. (3 m.) into the roof of the mains, while the other six were placed in the roof of the first entry of the panel.

Approximately 60% of the triggers received by the microseismic system during the 1.5 month retreat of Panel 2D were located using a simplex algorithm and produced a microseismic event. Issues with identifying the P-wave arrival took place during processing since triaxial geophones were unable to be installed. This significantly impacted finding event locations. Also, P- and S-wave velocities were estimated, as calibration events for the system were not able to be performed. Approximately 21% of the events during retreat were "well-located" with errors less than 100 ft. (30.5 m.), but processing results indicate that there is little confidence in them being true locations. It was found that data still provided an accurate location with respect to the nearest crosscut by comparing event clusters to approximate face locations. As the panel retreated, results show a definitive cluster of events progressing outby. It is expected that these clusters occur in the front abutment of the retreat.

Although confidence was low in the location and magnitudes after processing the data, event rates could still be analyzed. Results indicated that peaks in the hourly event rate frequently occurred once in the early morning hours during the mine's maintenance shift, and again in the afternoon during one of the two production shifts. Rates typically exponentially grew from a base level around the late evening hours, through the first smaller peak of events in the morning, and until the larger peak in the afternoon. After the large hourly peak in events, rates sharply dropped. A very large peak of 444 events was observed between 5:00 pm and 6:00 pm EST on March 26<sup>th</sup>. A large section of hanging roof could have failed, possibly causing the

large peak in events per hour, but documentation of individual caving events was not available from the mine site. The five day pause in retreat between March 16<sup>th</sup> and 20<sup>th</sup> would not be expected to influence this high event rate, as pillaring began again six days before the spike.

Results also show a disparity in event rates when retreating under a shale roof as opposed to under a sandstone/sandy shale roof. The average event rate was much higher between March 2<sup>nd</sup> and 8<sup>th</sup> when retreating under shale than it was between March 11<sup>th</sup> and 15<sup>th</sup> when retreating under a mixture of sandstone and sandy shale. Shale roof is more brittle than a sandstone roof, which would account for a higher rate of events. No conclusions could be made when retreating under 1,000 ft. (305 m.) of cover because of inconsistent data collection and exact face locations being unknown.

Monitoring the development for Panel 2E yielded 550 events over approximately two months. On average, the moment magnitudes of development events were -0.61, as opposed to the average retreat event having a magnitude of -0.91. Coupling effects could have played a role in the difference of recorded magnitudes, but more data is needed for determination. Minimum and maximum magnitudes were roughly the same between retreat and development.

The development of Panel 2E was more sparsely monitored than the previous panel's retreat. Only 60% of the period between April 10<sup>th</sup> and June 17<sup>th</sup> was monitored. As a result, event rates were missing for large periods of time. Results indicated that hourly event rates were higher during the first few days of monitoring, with peaks occurring above 10 events per hour. This is possibly due to the stress still redistributing across Panel 2D. The rest of the monitoring period resulted in no hourly event rates higher than 10, and only two hours with activity greater than five events.

### ***3.11 Future Work and Uses***

Once Panel 2E is fully developed and prepared for retreat, efforts will be taken to install five uniaxial and two triaxial geophones 10 ft. (3 m.) into the roof of the first entry of the panel, furthest away from the previous barrier pillar. The triaxial geophones will assist in receiving the P-wave coming from the microseismic sources induced by caving. Multiple calibration events will be performed, once before retreat begins, and twice during retreat to input more accurate P- and S-wave velocities to help determine event locations. Borehole pressure cells (BPCs) will be installed in pillars left between the first two entries that are under 1,000 ft. (305 m.) of cover to

determine their loading during retreat. Photogrammetry work, where photos are taken to determine any dimensional changes, will be completed on the pillars monitored by BPCs to compare to loading and recorded microseismic events.

The overall objective of performing various monitoring techniques is to adequately understand the ground response during the retreat of a coal mine panel. With additional microseismic recording and improved data, a detailed examination of the stress redistribution and creation of rock failures can be undertaken. The mine operator for this site will be able to use the gathered data for hazard mitigation and improve safety and ground stability by identifying problematic zones. Pillar sizes may be optimized and certain geologic hazards may be avoided.

# **Chapter 4: Summary of Results and Conclusions**

## **4.1 Results and Conclusions**

A room and pillar mine panel in the Jawbone coal seam in Southwest Virginia was monitored for microseismicity during retreat. Roughly one-third of the development of the mine section's subsequent panel was monitored as well. Eight uniaxial geophones were used to record events. Two were placed 10 ft. (3 m.) into the roof of the mains, while the other six were placed in the roof of the first entry of the panel.

Approximately 60% of the triggers received by the microseismic system during the 1.5 month retreat of Panel 2D were located using a simplex algorithm and produced a microseismic event. Issues with identifying the P-wave arrival took place during processing since triaxial geophones were unable to be installed. This significantly impacted finding event locations. Also, P- and S-wave velocities were estimated, as calibration events for the system were not able to be performed. Approximately 21% of the events during retreat were "well-located" with errors less than 100 ft. (30.5 m.), but processing results indicate that there is little confidence in them being true locations. It was found that data still provided an accurate location with respect to the nearest crosscut by comparing event clusters to approximate face locations. As the panel retreated, results show a definitive cluster of events progressing outby. It is expected that these clusters occur in the front abutment of the retreat.

Although confidence was low in the location and magnitudes after processing the data, event rates could still be analyzed. Results indicated that peaks in the hourly event rate frequently occurred once in the early morning hours during the mine's maintenance shift, and again in the afternoon during one of the two production shifts. Rates typically exponentially grew from a base level around the late evening hours, through the first smaller peak of events in the morning, and until the larger peak in the afternoon. After the large hourly peak in events, rates sharply dropped. A very large peak of 444 events was observed between 5:00 pm and 6:00 pm EST on March 26<sup>th</sup>. A large section of hanging roof could have failed, possibly causing the large peak in events per hour, but documentation of individual caving events was not available from the mine site. The five day pause in retreat between March 16<sup>th</sup> and 20<sup>th</sup> would not be expected to influence this high event rate, as pillaring began again six days before the spike.

Results also show a disparity in event rates when retreating under a shale roof as opposed to under a sandstone/sandy shale roof. The average event rate was much higher between March 2<sup>nd</sup> and 8<sup>th</sup> when retreating under shale than it was between March 11<sup>th</sup> and 15<sup>th</sup> when retreating under a mixture of sandstone and sandy shale. Shale roof is more brittle than a sandstone roof, which would account for a higher rate of events. No conclusions could be made when retreating under 1,000 ft. (305 m.) of cover because of inconsistent data collection and exact face locations being unknown.

Monitoring the development for Panel 2E yielded 550 events over approximately two months. On average, the moment magnitudes of development events were -0.61, as opposed to the average retreat event having a magnitude of -0.91. Coupling effects could have played a role in the difference of recorded magnitudes, but more data is needed for determination. Minimum and maximum magnitudes were roughly the same between retreat and development.

The development of Panel 2E was more sparsely monitored than the previous panel's retreat. Only 60% of the period between April 10<sup>th</sup> and June 17<sup>th</sup> was monitored. As a result, event rates were missing for large periods of time. Results indicated that hourly event rates were higher during the first few days of monitoring, with peaks occurring above 10 events per hour. This is possibly due to the stress still redistributing across Panel 2D. The rest of the monitoring period resulted in no hourly event rates higher than 10, and only two hours with activity greater than five events.

## ***4.2 Future Work and Recommendations***

Further monitoring will take place during the retreat of Panel 2E. A total of seven geophones will be connected to the previous system. Four uniaxial and two triaxial geophones will be installed along the roof of the entry furthest from the latest barrier pillar. Figure 34 displays where the geophones will be located in accordance with the panel. These additional sensors will create an array that surrounds the future gob area of Panel 2E. The use of triaxial geophones will greatly increase the accuracy and precision in locating mining induced microseismic events, but results will still be limited because of the two dimensional array. Flash drives connected to the data recorders will again be used. Data collection during this period though is expected to be more regimented, with defined days of flash drive recovery.

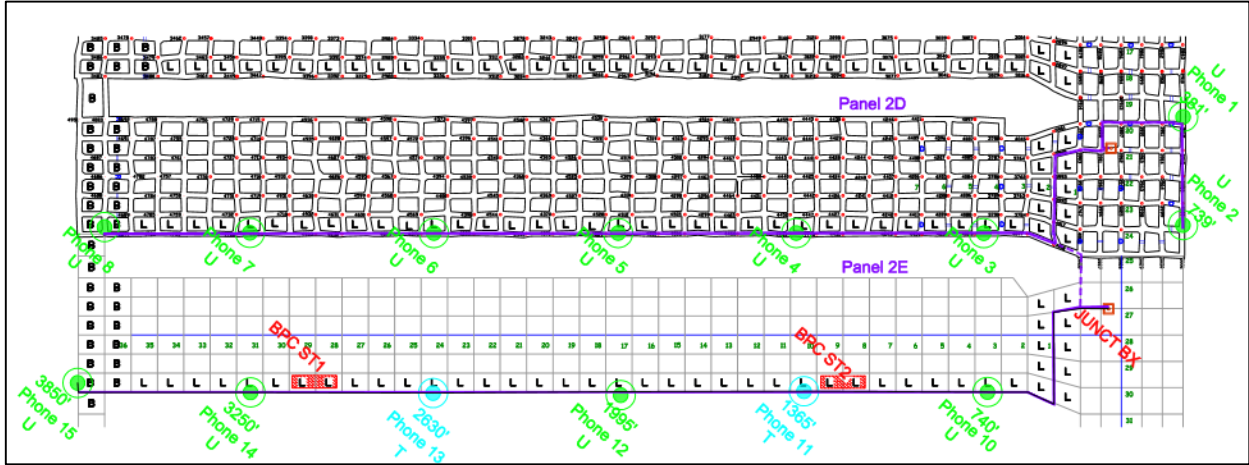


Figure 34: Future microseismic and borehole pressure cell monitoring.

If possible, geophones should be placed in a three-dimensional array around a targeted monitoring area. In order for this to take place in a coal mine, geophones must be placed on the surface in addition to the roof of the panel. Data obtained underground would need to be transferred above ground through a medium such as a fiber cable to be synched to the geophones on the surface. Without the synchronization, two independent sets of events would be found that would be difficult to compare.

Several calibration events will be performed on the surface to obtain more accurate wave velocities during the retreat of Panel 2E. These events will have a known time, magnitude, and location, and will allow more confidence in mining induced microseismic event locations. Calibrations will occur once at the beginning of retreat and twice during the retreat. Daily calibrations would be optimum, since the rockmass is constantly changing during retreat, but due to costs and equipment availability only three calibration sessions will be performed.

Borehole pressure cells (BPCs) will also be installed in pillars left between the first two entries of Panel 2E. Two stations, one near crosscut 9 and the other near crosscut 29, will monitor the change in pillar loading as the retreat line passes. Each station will comprise of two monitored pillars, each with two installed BPCs. One BPC will be placed directly in the center of the pillars at 25 ft. (7.6 m.) deep, while the other will be installed a quarter of the way into the pillars at 12.5 ft. (3.8 m.) deep. Each station is under the panel's deepest cover at approximately 1,000 ft. (305 m.). The BCPs will be connected to a permissible data recorder since they will be placed in the panel's return air. Data is able to be retrieved from the chosen data recorder

wirelessly as long as there is a “line-of-sight” to the device. Figure 35 displays the BPC layout near crosscut 9.

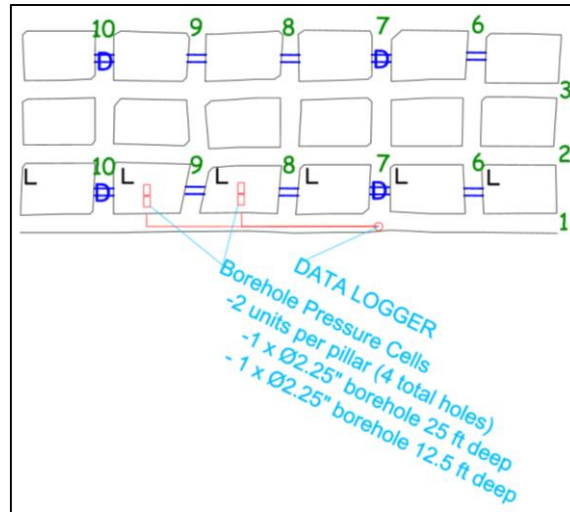


Figure 35: BPC monitoring layout.

In addition to BPC monitoring, photogrammetry work will be performed on the pillars installed with pressure cells. Photogrammetry refers to the process of taking photos of an object over time to computationally monitor any changes. Specifically in a mine site, changes refer to mechanisms such as pillar expansion, spalling, and entry deformation. Observations obtained from the photographs will be able to be compared with quantitative data obtained from the BPCs. Gathered data from the BPCs and photogrammetry work will be analyzed to determine any correlation with recorded microseismic events occurring during the panel’s retreat.

The overall objective of performing various monitoring methods is to obtain a better idea for the ground response during the retreat of a coal mine panel. With additional microseismic recording and improved data, a detailed examination of the stress redistribution and creation of rock failures for a retreat coal mine panel can be undertaken. The mine operator for this site will be able to use the gathered data for hazard mitigation and improve safety and ground stability by identifying zones of instability. Pillar sizes may be optimized and certain geologic hazards may be avoided.

## References

- Alber, M., Fritschen, R., Bischoff, M., & Meier, T. (2009). Rock mechanical investigations of seismic events in a deep longwall coal mine. *International Journal of Rock Mechanics and Mining Sciences*, 46(2), 408–420.
- AMSS - Analysis of Multiple Seam Stability (Version: 2.1.02) [Software]. (2013). Pittsburgh, PA: U.S. Department of Health and Human Services, Public Health Service, Centers for Disease Control and Prevention, National Institute for Occupational Safety and Health
- ARMPS - Analysis of Retreat Mining Pillar Stability (Version: 6.2.02) [Software]. (2013). Pittsburgh, PA: U.S. Department of Health and Human Services, Public Health Service, Centers for Disease Control and Prevention, National Institute for Occupational Safety and Health
- Bourbié, T. (1987). Acoustics of porous media. Paris: Editions Technip, pp. 240.
- Campoli, A. A., Oyler, D. C., & Chase, F. E. (1989). Performance of a novel bump control pillar extracting technique during room-and-pillar retreat coal mining. US Department of the Interior, Bureau of Mines.
- Campoli, A., Kertis, C., & Goode, C. (1987). Coal Mine Bumps: Five Case Studies in the Eastern United States. NIOSH Information Circular. Pittsburgh, PA: U.S. Department of the Interior, Bureau of Mines, NTIS PB90-265505, IC 9149, 1-34.
- Chase, F. E., Mark, C., & Heasley, K. A. (2002). Deep cover pillar extraction in the US coalfields. *Proceedings of the 21th International Conference on Ground Control in Mining*, Morgantown, WV, 69–80.
- CSM. (n.d.). Coal Mining Methods. Colorado School of Mines. Retrieved July 10, 2015, from <http://emfi.mines.edu/emfi2011/Coal Mining Methods - EMFI Summary.pdf>
- Descour, J.M. & Miller, R.J. (1987) Coal Mine Bump Monitoring. Contract J0245009, CO Sch. Mines. USBM OFR 32-88, 111; NTIS PB88-214309/AS
- Ellenberger, J., Heasley, K., Swanson, P., & Mercier, J. (2001). Three dimensional microseismic monitoring of a Utah longwall. *Rock Mechanics in the National Interest, Vol II*. Lisse, Netherlands, 1321-1326.
- Gale, W., Heasley, K., Iannacchione, A., Swanson, P., Hatherly, P., King, A., & others. (2001). Rock damage characterisation from microseismic monitoring. *Rock Mechanics in the National Interest, Vol II*. Lisse, Netherlands, 1313-1320.
- Ghasemi, E., Ataei, M., Shahriar, K., Sereshki, F., Jalali, S. E., & Ramazanzadeh, A. (2012). Assessment of roof fall risk during retreat mining in room and pillar coal mines. *International Journal of Rock Mechanics and Mining Sciences*, 54, 80–89.

- Hazzard, J. & Young, R. (2004). Dynamic modelling of induced seismicity. *International Journal of Rock Mechanics and Mining Sciences*, 41(8), 1365–1376.
- Heasley, K. A., Ellenberger, J. L., & Jeran, P. W. (2001). An analysis of rock failure around a deep longwall using microseismics. *Proceedings of the 20th International Conference on Ground Control in Mining*, Morgantown, WV, 280–286.
- Hyperion Software Suite. Vers. 16.0. Engineering Seismology Group. N.p.: n.p., 2014. Program documentation.
- Iannacchione, A., Esterhuizen, G., Bajpayee, T., Swanson, P., Chapman, M., & others. (2005). Characteristics of mining-induced seismicity associated with roof falls and roof caving events. *The 40th US Symposium on Rock Mechanics (USRMS)*, Anchorage, AK.
- Luo, X., Hatherly, P., & McKavanagh, B. (1998). Microseismic Monitoring of a Longwall Caving Process at Gordonstone Mine, Australia. *Advances in Rock Mechanics*, 67-79.
- Luxbacher, K., Westman, E., & Swanson, P. (2007). Time-lapse tomography of a longwall panel: A comparison of location schemes. *26th International Conference on Ground Control in Mining*, Morgantown, WV.
- Mark, C. (1990). Pillar Design Methods for Longwall Mining. USBM IC 9247, 53.
- Mark, C. (2009). Deep cover pillar recovery in the US. *Proceedings of the 28th International Conference on Ground Control in Mining*, Morgantown, WV, 1–9.
- Mark, C., Chase, F., & Pappas, D. (2003). Reducing the risk of ground falls during pillar recovery. *Transactions-Society for Mining Metallurgy and Exploration*, 314, 153–160.
- Mark, C., Karabin, G., Zelanko, J. C., Hoch, M. T., & Chase, F. (2002). Evaluation of pillar recovery in southern West Virginia. *Proceedings of the 21st International Conference on Ground Control in Mining*, Morgantown, WV, 81-89.
- Mark, C. & Molinda, G. (2007). Development and application of the coal mine roof rating (CMRR). *Proceedings of the International Workshop on Rock Mass Classification in Underground Mining, Information Circular* (Vol. 9498).
- Mark, C. & Tuchman, R. (1997). New Technology for Ground Control in Retreat Mining. U.S. Department of Health and Human Services, Public Health Service, Centers for Disease Control and Prevention, National Institute for Occupational Safety and Health Information Circular, Pittsburgh, PA, 1-129.
- MSHA. (2007). Crandall Canyon Mine Report of Investigation. Arlington, VA: US Department of Labor, Mine Safety and Health Administration, Coal Mine Safety and Health, Office of the Administrator.
- MSHA. (2015). Mining Industry Accident, Injuries, Employment, and Production Statistics and Reports. From <http://www.msha.gov/ACCINJ/accinj.htm>, accessed Jan 20th, 2015.

- NIOSH. (2010). Research Report on the Coal Pillar Recovery Under Deep Cover. US Department of Health and Human Services, Centers for Disease Control and Prevention, National Institute for Occupational Safety and Health, Office of Mine Safety and Health Research.
- Obert, L. & Duvall, W.I. (1967). *Rock Mechanics and the Design of Structures in Rock*. Wiley, New York, 449-459.
- Poulsen, B. (2010). Coal pillar load calculation by pressure arch theory and near field extraction ratio. *International Journal of Rock Mechanics and Mining Sciences*, 47(7), 1158–1165.
- Ren, G. & Li, J. (2008). A study of angle of draw in mining subsidence using numerical modeling techniques. *Electronic Journal of Geotechnical Engineering*, 13, 1–13.
- Spence, W., Sipkin, S., & Choy, G. (1989). Measuring the Size of an Earthquake. In *Earthquakes and Volcanos* (1st ed., Vol. 21). Golden, CO: U.S. Geological Survey. From <http://earthquake.usgs.gov/learn/topics/measure.php>, accessed Nov 11th, 2015.
- Swanson, P., Stewart, C., & Koontz, W. (2008). Monitoring Coal Mine Seismicity with an Automated Wireless Digital Strong-Motion Network. *Proceedings of the 27th International Conference on Ground Control in Mining*, Morgantown, WV, 79-86.
- Yavuz, H. (2004). An estimation method for cover pressure re-establishment distance and pressure distribution in the goaf of longwall coal mines. *International Journal of Rock Mechanics and Mining Sciences*, 41(2), 193–205.
- Zipf, R. K. (2001). Toward pillar design to prevent collapse of room-and-pillar mines. *108th Annual Exhibit and Meeting, Society for Mining, Metallurgy and Exploration*, Denver, CO.

## Appendix A: Source Parameter Formulas

### Variables:

$\alpha$  = P-wave velocity

$\beta$  = S-wave velocity

$c$  = notation for P- or S-wave velocity

$r$  = rock density

$\mu$  = shear modulus

$v_{max}$  = max velocity recorded from root-mean square trace

$\alpha_{max}$  = max acceleration recorded from root-mean square trace

$R$  = hypocentral distance

### Source Size and Displacement (Hyperion, 2014):

$$\text{Seismic Moment} = M_0 = \frac{4\pi\rho_0 c_0^3 R \Omega_0 c}{F_c}$$

$$\text{Moment Magnitude} = M = \frac{2}{3} \log M_0 - 6.0$$

$$\text{Energy Release} = E_0 = 4\pi\rho c R^2 S_{V2c}$$

$$\text{Source Radius} = r_0 = \frac{K_c \beta}{2\pi f_c}$$

### Stress Release Estimates (Hyperion, 2014):

$$\text{Static Stress Drop} = \Delta\sigma = \frac{7M_0}{16r_0^3}$$

$$\text{Apparent Stress} = \sigma_a = \frac{\mu E_0}{M_0}$$

$$\text{Dynamic Stress Drop} = \Delta\sigma_d = 2.50\rho R\alpha_{max}$$

### Ground Motion Parameters and Efficiency (Hyperion, 2014):

$$\text{Peak Velocity Parameter} = PVP = Rv_{max}$$

$$\text{Peak Acceleration Parameter} = PAP = \rho R\alpha_{max}$$

# Appendix B: Estimated Timing

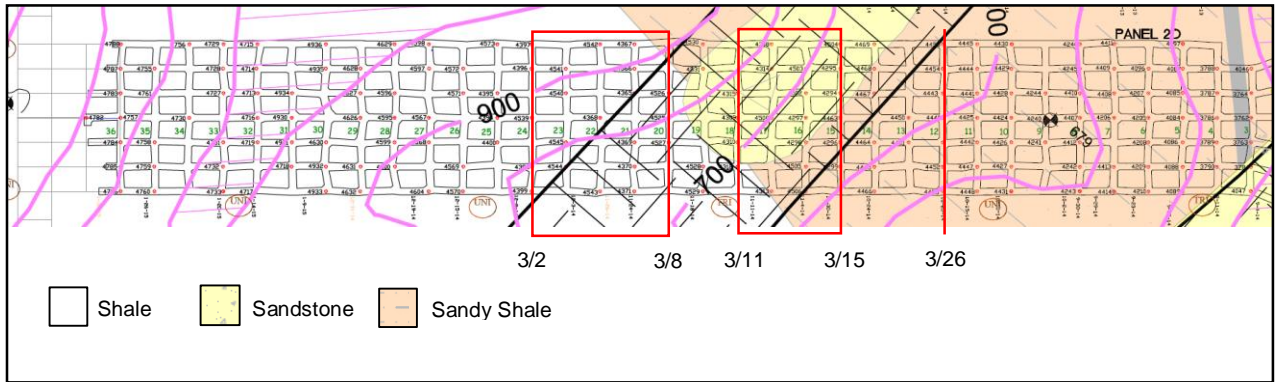


Figure B-1: Estimated face locations with reference to roof geology and depth of cover.

# Appendix C: Event Rate Comparison T-Test (3/02-3/08 and 3/11-3/15)

Hourly Event Rate:

**Means:**

$\mu_1$  = Hourly event rate from March 2<sup>nd</sup> to March 8<sup>th</sup>

$\mu_2$  = Hourly event rate from March 11<sup>th</sup> to March 15<sup>th</sup>

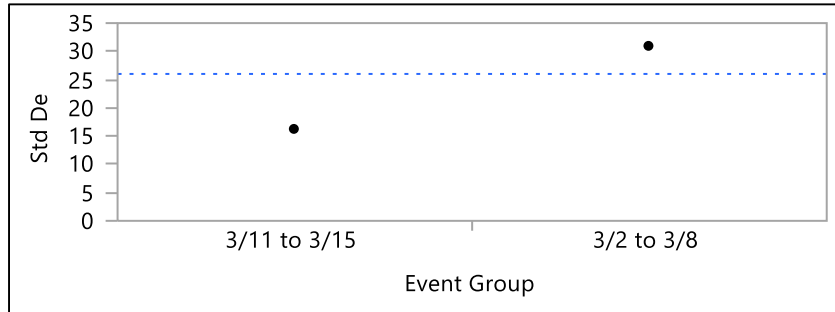
**Hypotheses:**

$$H_0: \mu_1 \leq \mu_2 \quad H_a: \mu_1 > \mu_2$$

**Analysis:**

$$\frac{s_{max}}{s_{min}} = \frac{947.6}{256.5} > 2 \therefore \text{Welch's } T - \text{Test}$$

### Tests that the Variances are Equal



Level	Count	Std Dev	MeanAbsDif to Mean	MeanAbsDif to Median
3/11 to 3/15	98	16.01614	11.53145	10.78571
3/2 to 3/8	151	30.78328	21.94939	19.98013

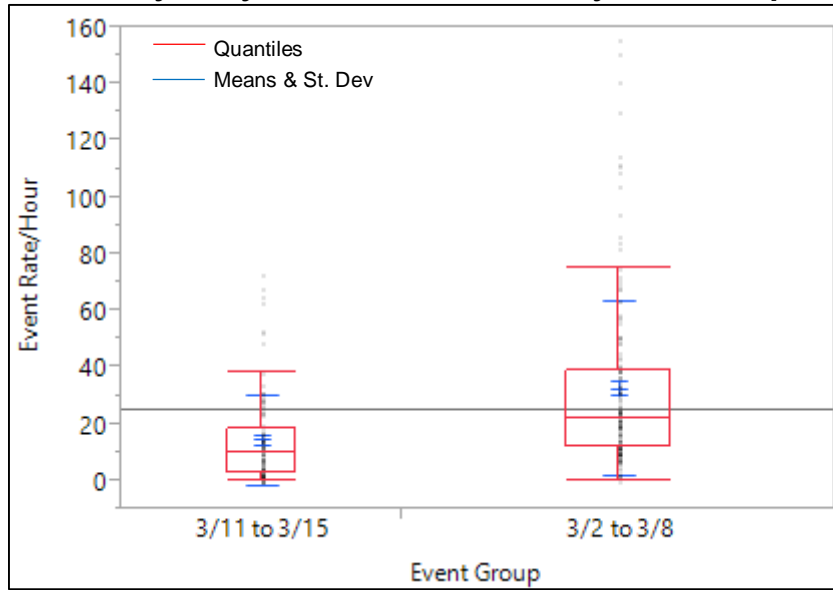
Test	F Ratio	DFNum	DFDen	p-Value
O'Brien[.5]	8.4578	1	247	0.0040*
Brown-Forsythe	10.8715	1	247	0.0011*
Levene	19.6098	1	247	<.0001*
Bartlett	43.2205	1	.	<.0001*
F Test 2-sided	3.6941	150	97	<.0001*

### Welch's Test

Welch Anova testing Means Equal, allowing Std Devs Not Equal

F Ratio	DFNum	DFDen	Prob > F
36.3325	1	237.37	<.0001*
t Test			
6.0276			

### Oneway Analysis of Event Rate/Hour By Event Group



### Means and Standard Deviations

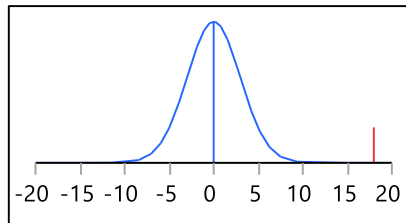
Level	Number	Mean	Std Dev	Std Err Mean	Lower 95%	Upper 95%
3/11 to 3/15	98	14.5612	16.0161	1.6179	11.350	17.772
3/2 to 3/8	151	32.5364	30.7833	2.5051	27.587	37.486

### T-Test

3/2-3/8 : 3/11-3/15

Assuming unequal variances

Difference	17.9752	t Ratio	6.027643
Std Err Dif	2.9821	DF	237.3668
Upper CL Dif	23.8500	Prob >  t	<.0001*
Lower CL Dif	12.1004	Prob > t	<.0001*
Confidence	0.95	Prob < t	1.0000



\*Calculations performed with JMP statistical software from SAS.

### Conclusion:

With a probability of less than 0.001, we can reject  $H_0$  and conclude that the hourly event rate from March 2<sup>nd</sup> to March 8<sup>th</sup> is higher than the hourly event rate between March 11<sup>th</sup> and March 15<sup>th</sup>.

## Moment Magnitude:

### Means:

$\mu_1$  = Moment Magnitudes of events between March 2<sup>nd</sup> and March 8<sup>th</sup>

$\mu_2$  = Moment Magnitudes of events between March 11<sup>th</sup> and March 15<sup>th</sup>

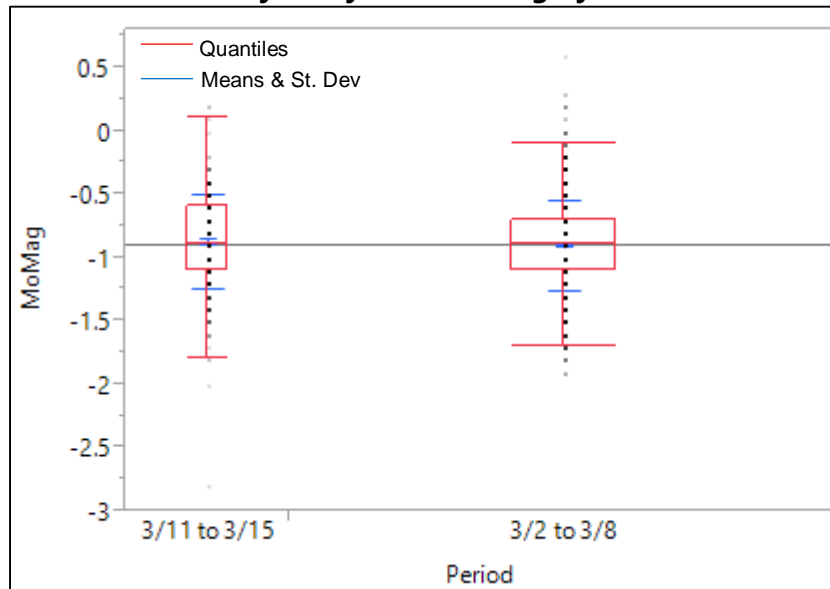
### Hypotheses:

$$H_0: \mu_1 = \mu_2 \quad H_a: \mu_1 \neq \mu_2$$

### Analysis:

$$\frac{s_{max}}{s_{min}} = \frac{0.139}{0.131} < 2 \quad \therefore \text{Pooled } T - \text{Test}$$

### Oneway Analysis of MoMag By Period



### Oneway Anova Summary of Fit

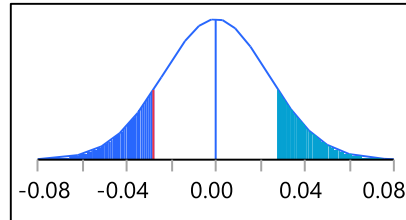
Rsquare	0.001038
Adj Rsquare	0.000301
Root Mean Square Error	0.365086
Mean of Response	-0.89712
Observations (or Sum Wgts)	1356

### t Test

3/2 to 3/8-3/11 to 3/15

Assuming equal variances

Difference	-0.02798	t Ratio	-1.1864
Std Err Dif	0.02358	DF	1354
Upper CL Dif	0.01828	Prob >  t	0.2357
Lower CL Dif	-0.07424	Prob > t	0.8822
Confidence	0.95	Prob < t	0.1178



### Analysis of Variance

Source	DF	Sum of Squares	Mean Square	F Ratio	Prob > F
Period	1	0.18761	0.187607	1.4075	0.2357
Error	1354	180.47118	0.133287		
C. Total	1355	180.65878			

### Means and Std Deviations

Level	Number	Mean	Std Dev	Std Err Mean	Lower 95%	Upper 95%
3/11 to 3/15	311	-0.87556	0.373364	0.02117	-0.9172	-0.8339
3/2 to 3/8	1045	-0.90354	0.362591	0.01122	-0.9256	-0.8815

### Means for Oneway Anova

Level	Number	Mean	Std Error	Lower 95%	Upper 95%
3/11 to 3/15	311	-0.87556	0.02070	-0.9162	-0.8350
3/2 to 3/8	1045	-0.90354	0.01129	-0.9257	-0.8814

\*Std Error uses a pooled estimate of error variance

### Conclusion:

With a probability value of 0.23, we fail to reject  $H_0$  and conclude that the moment magnitudes of events from March 2nd to March 8th equal the moment magnitudes of events between March 11th and March 15th.

## Appendix D: Descriptive Statistics of Processed Events

	<u>MoMag</u>		<u>Phones</u>		<u>Error</u>	
2D	Mean	-1.511	Mean	4.247	Mean	310.487
	Standard Error	0.020	Standard Error	0.009	Standard Error	2.218
	Median	-1	Median	4	Median	249.9
	Mode	-1	Mode	4	Mode	0
	Standard Deviation	2.297	Standard Deviation	1.073	Standard Deviation	254.624
	Sample Variance	5.274	Sample Variance	1.151	Sample Variance	64833.367
	Kurtosis	9.102	Kurtosis	0.054	Kurtosis	0.136
	Skewness	-3.264	Skewness	0.749	Skewness	0.931
	Range	11.9	Range	5	Range	1270.25
	Minimum	-9.9	Minimum	3	Minimum	0
	Maximum	2	Maximum	8	Maximum	1270.25
	Sum	-19918	Sum	55978	Sum	4092523.35
Count	13181	Count	13181	Count	13181	
Filtered (E<100 ft) 2D	Mean	-0.911	Mean	4.260	Mean	56.580
	Standard Error	0.007	Standard Error	0.020	Standard Error	0.414
	Median	-0.9	Median	4	Median	56.825
	Mode	-1.1	Mode	4	Mode	72.61
	Standard Deviation	0.361	Standard Deviation	1.026	Standard Deviation	21.783
	Sample Variance	0.131	Sample Variance	1.053	Sample Variance	474.516
	Kurtosis	1.030	Kurtosis	-0.105	Kurtosis	-0.747
	Skewness	0.339	Skewness	0.635	Skewness	-0.020
	Range	3.5	Range	5	Range	89.91
	Minimum	-2.8	Minimum	3	Minimum	10.08
	Maximum	0.7	Maximum	8	Maximum	99.99
	Sum	-2523.9	Sum	11800	Sum	156726.14
Count	2770	Count	2770	Count	2770	
2E	Mean	-1.468	Mean	3.699	Mean	488.890
	Standard Error	0.115	Standard Error	0.029	Standard Error	14.297
	Median	-0.8	Median	4	Median	521
	Mode	-9.9	Mode	4	Mode	999.9
	Standard Deviation	2.606	Standard Deviation	0.649	Standard Deviation	324.440
	Sample Variance	6.790	Sample Variance	0.421	Sample Variance	105261.405
	Kurtosis	6.300	Kurtosis	0.827	Kurtosis	-1.024
	Skewness	-2.786	Skewness	0.646	Skewness	0.076
	Range	10.9	Range	4	Range	1502.87
	Minimum	-9.9	Minimum	3	Minimum	0
	Maximum	1	Maximum	7	Maximum	1502.87
	Sum	-755.8	Sum	1905	Sum	251778.42
Count	515	Count	515	Count	515	
Filtered (E<100 ft) 2E	Mean	-0.620	Mean	3.967	Mean	55.392
	Standard Error	0.069	Standard Error	0.093	Standard Error	2.985
	Median	-0.7	Median	4	Median	54.13
	Mode	-0.7	Mode	4	Mode	60.28
	Standard Deviation	0.538	Standard Deviation	0.730	Standard Deviation	23.314
	Sample Variance	0.289	Sample Variance	0.532	Sample Variance	543.538
	Kurtosis	1.730	Kurtosis	3.807	Kurtosis	-0.872
	Skewness	0.532	Skewness	1.116	Skewness	0.215
	Range	3.2	Range	4	Range	88.44
	Minimum	-2.2	Minimum	3	Minimum	10.96
	Maximum	1	Maximum	7	Maximum	99.4
	Sum	-37.8	Sum	242	Sum	3378.92